Journal of
Medicinal Chemistry

Article

A SCAFFOLD SIMPLIFICATION STRATEGY LEADS TO A NOVEL GENERATION OF DUAL HUMAN IMMUNODEFICIENCY VIRUS AND ENTEROVIRUS-A71 ENTRY INHIBITORS

Belén Martínez-Gualda, Liang Sun, Olaia Martí-Marí, Sam Noppen, Rana Abdelnabi, Carol M. Bator, Ernesto Quesada, Leen Delang, Carmen Mirabelli, Hyunwook Lee, Dominique Schols, Johan Neyts, Susan Hafenstein, María-José Camarasa, Federico Gago, and ANA SAN-FELIX

J. Med. Chem., **Just Accepted Manuscript** • DOI: 10.1021/acs.jmedchem.9b01737 • Publication Date (Web): 06 Dec 2019

A SCAFFOLD SIMPLIFICATION STRATEGY LEADS TO A NOVEL GENERATION OF DUAL HUMAN IMMUNODEFICIENCY VIRUS AND ENTEROVIRUS-A71 ENTRY INHIBITORS

*Belén Martínez-Gualda[1a¥], Liang Sun[2b¥], Olaia Martí-Marí[1], Sam Noppen[2], Rana Abdelnabi[2], Carol M. Bator[4], Ernesto Quesada[1], Leen Delang[2], Carmen Mirabelli[2c], Hyunwook Lee[4], Dominique Schols[2], Johan Neyts[2], Susan Hafenstein[4,5], María-José Camarasa[1], Federico Gago[3], Ana San-Félix[*1]*

[1] Instituto de Química Médica (IQM-CSIC), 28006 Madrid, Spain

[2]University of Leuven, Department of Microbiology and Immunology, Rega Institute for Medical Research, Laboratory of Virology and Chemotherapy, B-3000 Leuven, Belgium

[3] Departamento de Ciencias Biomédicas y Unidad Asociada IQM-UAH, Universidad de Alcalá, E-28805 Alcalá de Henares, Madrid, Spain

[4] Department of Biochemistry and Molecular Biology, Huck Institutes of the Life Sciences, the Pennsylvania State University, University Park, 16802 Pennsylvania, USA

[5] Department of Medicine, the Pennsylvania State University College of Medicine, Hershey, 17033 Pennsylvania, USA

Keywords: Antivirals; HIV; EV71; Tryptophan; indole; palladium-catalyzed C-H activation

ABSTRACT

Currently there are only three FDA-approved drugs that inhibit HIV entry-fusion into host cells. The situation is even worse for enterovirus EV71 infection for which no antiviral therapies are available. We describe here the discovery of potent entry dual inhibitors of HIV and EV71. These compounds contain in their structure three or four tryptophan (Trp) residues linked to a central scaffold. Critical for anti-HIV/EV71 activity is the presence of extra phenyl rings, bearing one or two carboxylates, at the C2 position of the indole ring of each Trp residue. The most potent derivatives, **22** and **30,** inhibit early steps of the replicative cycles of HIV-1 and EV-A71 by interacting with their respective viral surfaces (glycoprotein gp120 of HIV and 5-fold axis of the EV-A71 capsid). The high potency, low toxicity, facile chemical synthesis and great opportunities for chemical optimization make them useful prototypes for future medicinal chemistry studies.

INTRODUCTION

Human immunodeficiency virus (HIV) is a retrovirus that infects immune cells within the body. Without treatment the infection can result in the development of Acquired Immune Deficiency Syndrome (AIDS) and death. HIV infection affects more than 30 million people worldwide and caused about 1 million deaths in 2018.[1] Current antiretroviral therapy consists on more than 30 approved drugs or regimens. Although this therapy has significantly improved the quality of life of infected people, there is still no cure for the HIV infection.[2-7] Moreover, the combined therapy is lifelong, expensive, associated with significant side-effects/resistance, and not universally available in all regions of the world.[1,8-12] These limitations highlight the need for new lead compounds and/or novel therapeutic approaches to fight HIV infection.[13-17] In this regard, the initial steps in the HIV replicative cycle (entry and/or fusion with the host cells) are very attractive targets.[18-23] Despite their intrinsic interest there are only three entry inhibitors

approved by FDA, namely enfuvirtide[24,25] which targets the envelope glycoprotein gp41, maraviroc,[26] which targets the host cell receptor CCR5 and ibalizumab, an anti-CD4 humanized IgG4 monoclonal antibody.[27]

We have previously reported a family of tryptophan (Trp) dendrimers, exemplified by **1** (Fig. 1), that inhibit an early step in the replicative cycle of HIV by interacting with the gp120 glycoprotein of the viral envelope.[28] Interestingly, these compounds also proved to be potent inhibitors of the replication of the unrelated enterovirus 71 (EV71),[29] the virus responsible for most of the severe forms of hand, foot and mouth disease (HFMD). This virus is associated with neurological/cardiopulmonary complications and mortality in children below 5 years old.[30-34] In the last two decades, the increasing number of EV71 cases and the spread of the virus across Asia, followed by case reports in Spain, France, Germany and other European countries, have raised major concerns about its pandemic potential.[35-37]

Although a sub-genogroup C4 EV71-inactivated vaccine has been recently approved in China no antiviral therapies are so far, available for the prevention or treatment of EV71 infection.[38,39] Therefore, the development of effective and specific antiviral drugs is urgently needed.[40,41]

Remarkably, dendrimer **1** inhibits not only the laboratory BrCr strain of EV-A71 but also a large panel of clinical isolates (belonging to each of the genogroups) in the low-nanomolar/high-picomolar range.[29] Recently, it was demonstrated that **1** inhibits an early step in the replicative cycle of EV-A71 by targeting residues of the structural viral protein VP1, particularly the region that forms the 5-fold axis of the viral capsid, and thereby blocking the binding of the virus to the host cell.[42]

With respect to the SAR studies, modifications have been made in the central core, arms and periphery of the prototype **1.**[28,29,43,44] All of these modifications led to the conclusion that a

multivalent presentation of Trps, with their respective indole side chain and free carboxylates, is required to preserve the antiviral activity against both HIV and EV-A71.

The prototype **1** has a too high molecular weight (MW: 3576 Da) for drug development purposes. The aim of the present work is to develop compounds with smaller size retaining the same level of antiviral potency.

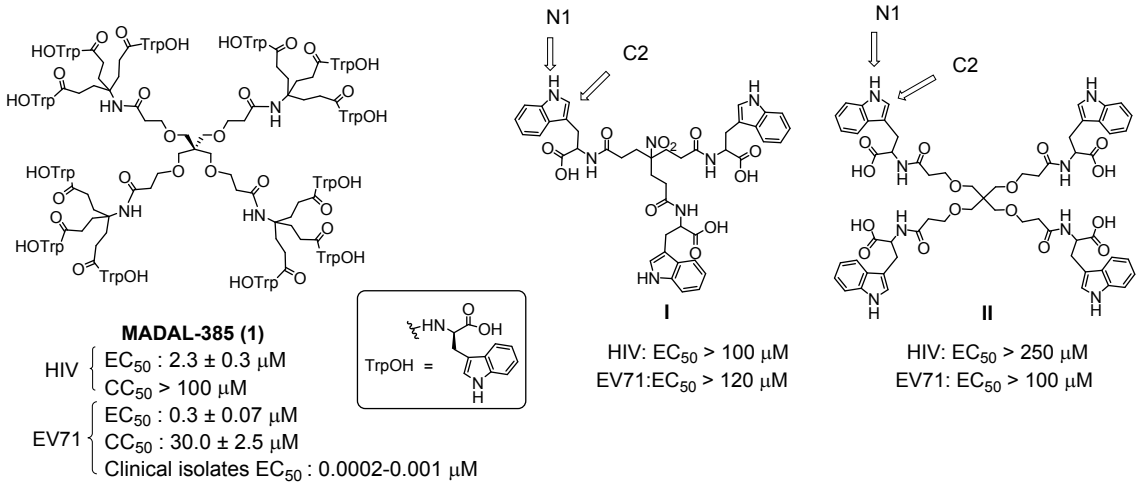

Figure 1. Structures of the prototype pentaerythritol derivative **MADAL-385 (1)** and "truncated" analogues **I** and **II**.

With this aim, a scaffold simplification strategy was applied and "truncated" analogues (**I** and **II**) of **1,** with only 3 or 4 Trps respectively (Figure 1), were firstly synthesized. However, as it will be later discussed in the Antiviral Evaluation section, both compounds resulted inactive against HIV and EV-A71.

Next, we decided to "decorate" **I** and **II** with moieties that could potentially participate in extra interactions with protein residues in the corresponding binding site. Phenyl rings functionalized with carboxylic groups were preferentially chosen because according to previous SAR studies, both aromaticity and negatively charged moieties are beneficial for anti-HIV and anti-EV-A71

activity.[43] Moreover, these functionalized phenyl rings could potentially participate in hydrogen bonding and/or hydrophobic/aromatic interactions with protein residues of the corresponding binding site. To introduce these substituents, we exploited the particular reactivity of the indole ring of Trp.[45] Thus, the C2 and N1 positions of the indole moiety were chosen as attachment points (Figure 1). Hereafter, we describe the synthesis, antiviral activities against HIV and EV71, and structure-activity relationships of this new generation of compounds.

RESULTS AND DISCUSSION

Chemistry

As mentioned, we designed truncated analogues of the prototype with extra functionalized aromatic rings attached to the C2 and N1 positions of the indole ring. We started with the synthesis of the tripodal derivatives **14–22** (Scheme 1), with functionalized phenyl rings on the C2 position of the indole ring of the three Trp residues. The synthesis of these compounds takes advantage of the methodology developed by Prof. Lavilla´s group which allows the direct C2 arylation of Trp and proteins containing this amino acid.[46,47] The reaction involves the simultaneous formation of new C-C bonds through a metal-catalyzed (Pd II) cross-coupling reaction.

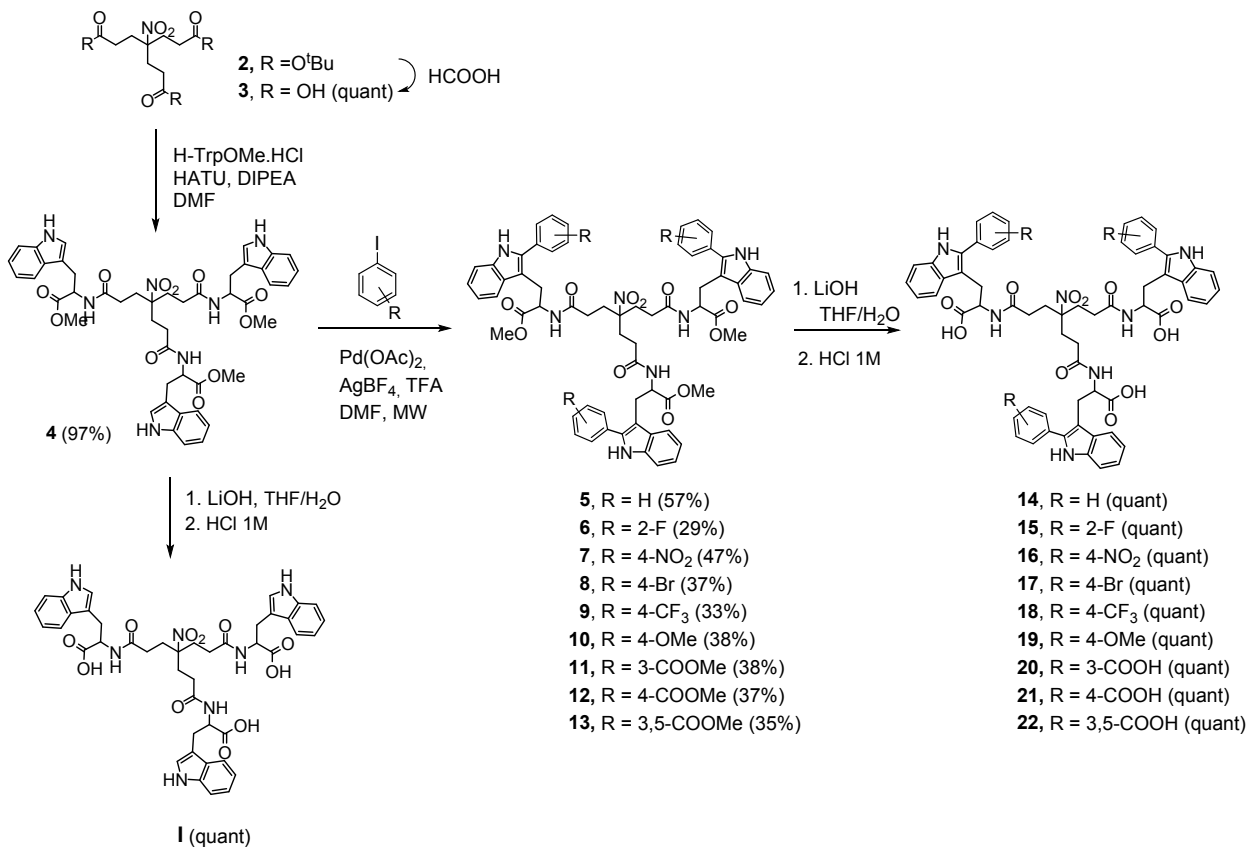

Scheme 1. Synthesis of the tripodal derivatives **I** and **14-22**.

The synthesis started with the commercially available scaffold **2**. Removal of the *t*-butyl protecting groups of **2**, followed by condensation of the resulting triacid (**3**)[48] with OMe protected Trp (H-TrpOMe·HCl) in the presence of HATU, as the coupling reagent, and DIPEA as the base, gave intermediate **4** (97%). The simultaneous chemoselective arylation on the C2 position of the three indole moieties of **4** was first attempted with phenyl iodide following Lavilla's conditions.[46,47] Overall, a mixture of 5 mol% $Pd(OAc)_2$, $AgBF_4$ (3 eq), TFA (3 eq), phenyl iodide (3 eq) in *N,N'*-dimethylformamide (DMF) was microwave (MW) irradiated at 80 ºC for 15 min. However, HPLC analysis revealed that only 5% of the desired compound **5** was present in the reaction mixture. The less lipophilic peaks were attributed to partial reaction in only one or two of the three Trps present in the starting compound **4**. However, the use of higher

temperatures (120 ºC), longer reaction times (30 min), excess of aryl iodide and $AgBF_4$ (2 eq for each Trp), allowed to finally obtain the desired methyl ester intermediate **5** with 57% yield. Saponification of the protecting ester moieties using $LiOH \cdot H_2O$ afforded the final compound **14** in quantitative yield (Scheme 1).

Next, and based on the good results obtained with phenyl iodide, the same synthetic methodology was applied with the other aryl iodides to afford compounds **6** (29%), **7** (47%), **8** (37%), **9** (33%), **10** (38%), **11** (38%), **12** (37%) and **13** (35%). These reactions proceed in remarkably short times (30 minutes), are completely selective (only reaction at C2 was observed) and compatible with ambient air/moisture. Methyl ester deprotection ($LiOH/H_2O$) of **6–13** afforded the final tripodal derivatives **15–22** in quantitative yields. In addition, the unsubstituted Trp derivative **I** was also prepared by deprotection of **4**.

The synthesis of the tetrapodal derivatives **28–30** was accomplished following a similar methodology as described for the tripodal series (Scheme 2). Again, the key step of the reaction involves the simultaneous formation of new C-C bonds through a metal-catalyzed (Pd II) cross-coupling reaction. In this case, the tetrapodal Trp derivative **24** was used as the starting material. In turn, this compound was obtained by condensation of the tetraacid **23**[49,50] with OMe-protected Trp (H-TrpOMe·HCl) in the presence of HATU as the coupling reagent and DIPEA as the base. Reaction of **24** with the corresponding aryl iodide, under the previously mentioned optimized conditions, afforded intermediates **25** (39%), **26** (32%) and **27** (26%), the subsequent deprotection ($LiOH/H_2O$) gave the desired final compounds **28–30** in quantitative yields. The C2 unsubstituted Trp derivative **II** was also prepared by deprotection ($LiOH/H_2O$) of **24**.

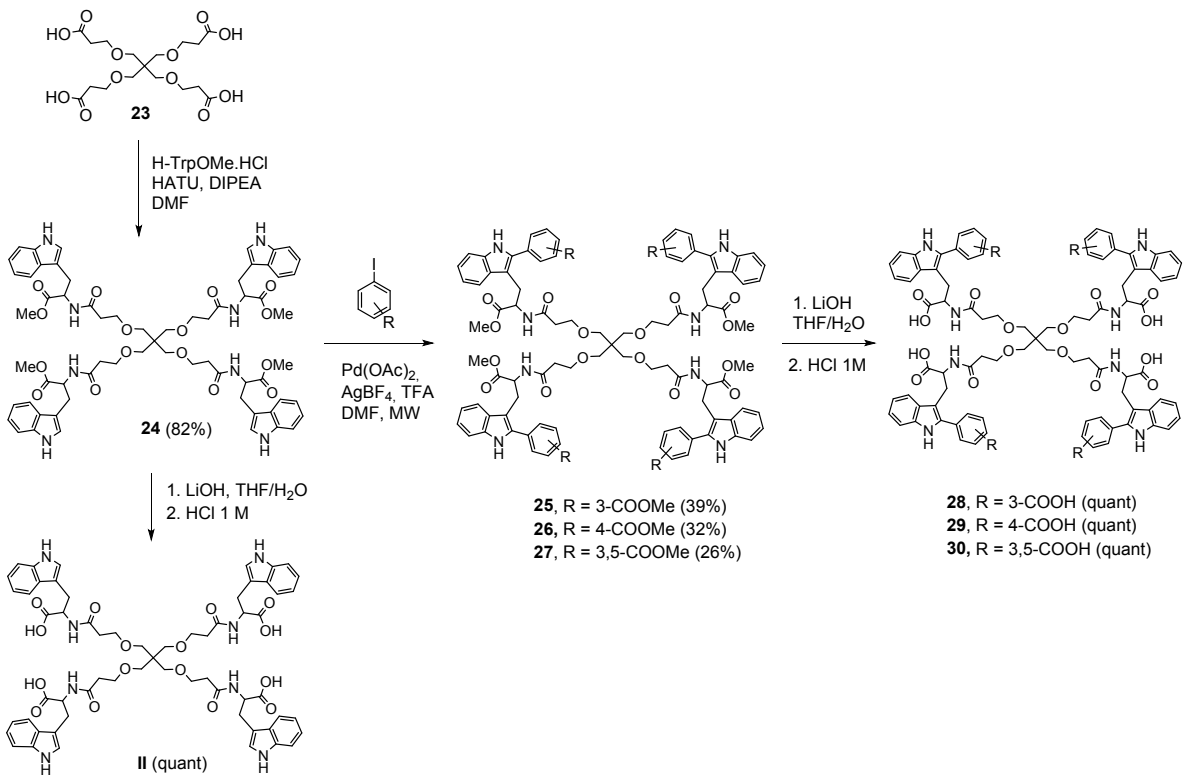

Scheme 2. Synthesis of the tetrapodal derivatives **II** and **28-30**.

Finally, to complete the SAR studies functionalized aromatic substituents at the N1 position of the indole moiety were introduced. Starting from **4**, the N1-substituted analogues **34–36** were synthesized by reaction with the corresponding benzyl bromides, in the presence of Cs_2CO_3 at 80 ºC followed by subsequent deprotection ($LiOH/H_2O$) of intermediates **31–33** (Scheme 3). The same synthetic methodology was applied to the synthesis of the tetrapodal analogue **38** which was obtained in 31% overall yield (Scheme 3).

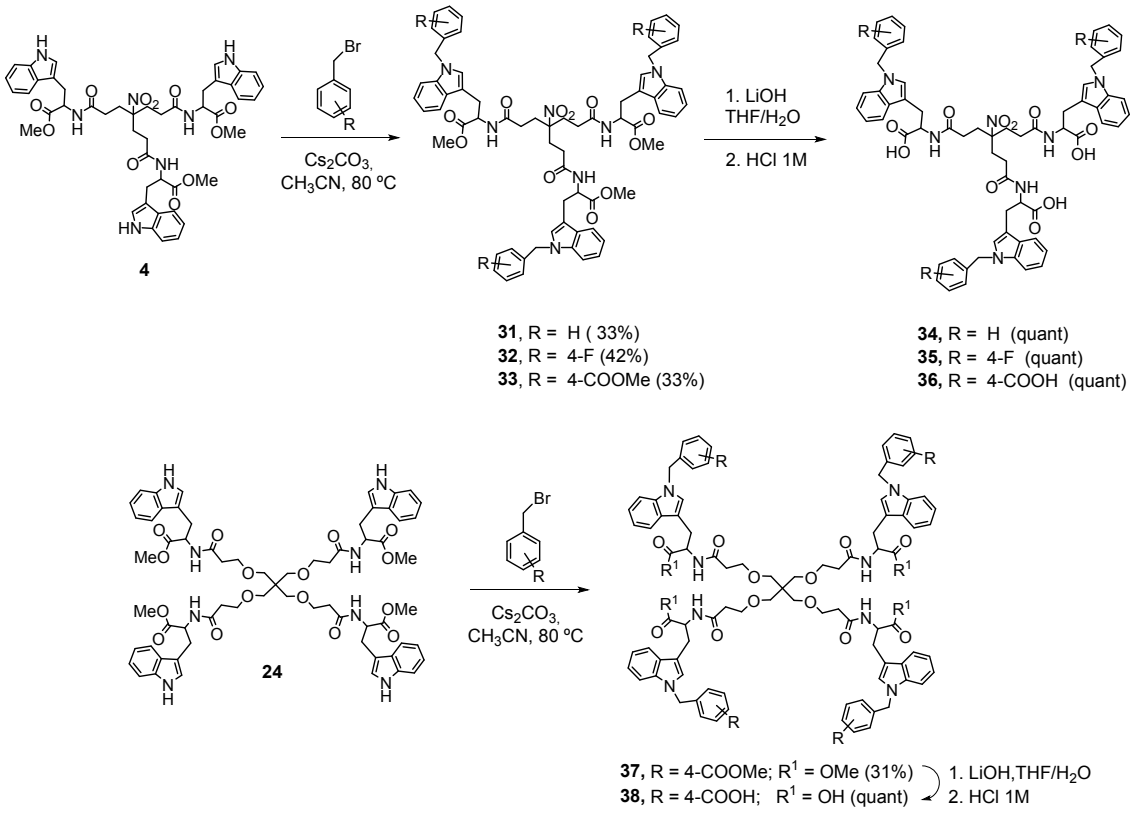

Scheme 3. Synthesis of the N1 substituted tripodal (**34–36)** and tetrapodal (**38)** derivatives.

As will be discussed later, compounds **22** and **30,** with isophthaloyl moieties at C2, were promising as anti-HIV and EV71 agents. To have access to higher amount of these compounds for further biological studies and structural modifications we explored a novel convergent synthetic strategy (Scheme 4) in which a C-2 arylated Trp derivative **41,** with a free amino group, was used as a key common intermediate.

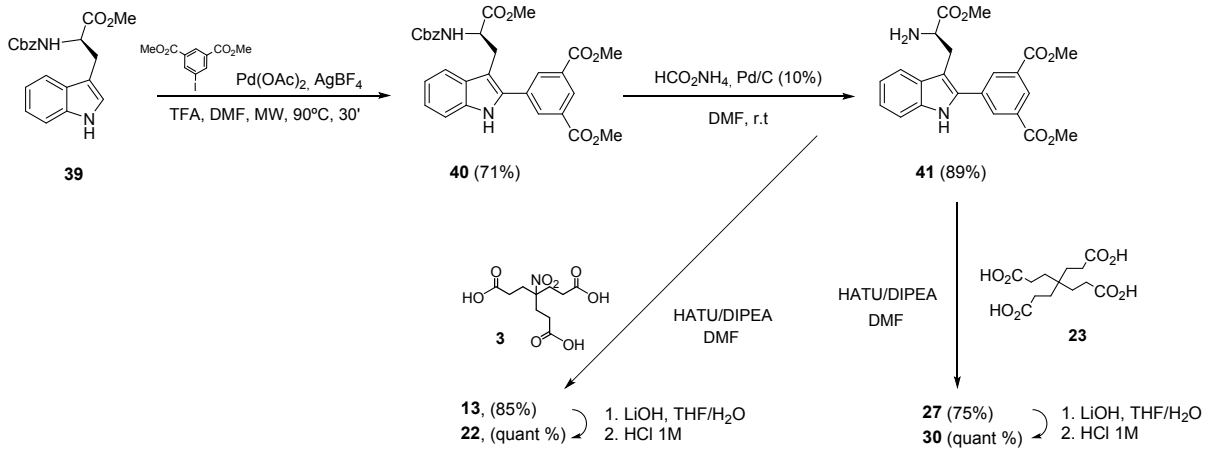

Scheme 4. Alternative synthetic route for the synthesis of **22** and **30**.

The synthesis of **41** started with the commercially available N^{α}-CBz tryptophan methyl ester (**39**) that was C-2 arylated with dimethyl 5-iodoisophthlate. The reaction was carried out in DMF as before, 5 mol% $Pd(OAc)_2$, $AgBF_4$, TFA, microwave irradiation during 30 min at 120 ºC, to afford intermediate **40** in good yield (71%). Subsequent carboxybenzyl (CBz) deprotection, was attempted first using hydrogen and 10% Pd/C. However, the starting compound was recovered intact. Instead, catalytic transfer hydrogenation using dry ammonium formate and 10% Pd/C[51] afforded the amino intermediate **41** in very good yield (89%). Further attachment of **41**, through the formation of amide bonds, to the tripodal (**3**) or tetrapodal (**23**) central scaffols afforded intermediates **13** (85%) and **27** (75%) respectively. Finally, methyl esther deprotection ($LiOH/H_2O$) afforded the desired final compounds **22** and **30** (structure in Scheme 1) in quantitative yields.

Compared to the divergent approach (Scheme 1), this convergent methodology enables de synthesis of **22** and **30** in a very simple and straightforward form. Moreover, the global yields of **22** and **30** improved considerably (54% *versus* 34% for **22**) and (47% *versus* 21% for **30**). Based

on these results we consider this second synthetic strategy as a general and more efficient approach for the synthesis of this type of tricyclic and tetracyclic Trp derivatives.

All the synthesized compounds were characterized by ^{1}H and ^{13}C NMR spectroscopies and High Resolution Mass Spectrometry (HRMS).

Antiviral evaluation

Antiviral activity against HIV

Compounds substituted at C2 (**14–22** and **28–30**) and N1 (**34–36** and **38**) positions of the indole moiety, together with the unsubstituted trimer **I** and tetramer **II**, were first evaluated for their inhibitory effects against HIV-1 and HIV-2 replication in cultured $CD4^{+}$ T cells (Table 1). The antiviral data of the prototype **1**, with 12 unsubstituted Trp residues on the periphery, is also included as a reference compound, as well as that of dextran sulfate-5000 (DS-5000) and pradimicin A (PRM-A). DS-5000 is a negatively charged HIV adsorption inhibitor[52] and PRM-A represents a gp120 carbohydrate-binding entry inhibitor.[53] These control compounds showed antiviral activities in the range previously reported.[52,53]

As shown in Table 1, the unsubstituted dendrimers **I** and **II** did not show any anti-HIV activity up to 100 μM. Besides, compounds **17** and **19**, with 4-Br-phenyl and 4-OMe-phenyl moieties, respectively, at C2 were also inactive at sub-toxic concentrations. However, compounds **14-16** and **18**, bearing phenyl, 2-F-phenyl, 4-NO_2-phenyl and 4-CF_3-phenyl moieties, respectively, at C2 showed modest but significant anti-HIV activity. Although the activity of these compounds was only moderate these data were important because they represented a first hint of activity in this series of compounds. Moreover, and taking into consideration that **I** and **II** did not exhibit

any antiviral activity against HIV, this result suggests that the C2 substituent may play an important role in the eventual antiviral activity.

Interestingly, the tripodal derivative **21**, with one COOH substituent in the *para* position of the phenyl ring (EC_{50} = 2.4 μM), was as active as the prototype **1** (EC_{50} = 2.3 μM) while the tripodal derivative **22**, with 2 COOHs at positions 3 and 5 of the phenyl ring (isophthaloyl moiety) was even better (EC_{50} = 0.27 μM). These data clearly demonstrate that the phenyl rings with free carboxylic acids on C2 play an important role in the anti-HIV activity.

Shifting the position of the substituted aromatic ring on the indole side-chain to N1 (compounds **34–36** and **38**) led to a substantial decrease of antiviral activity. This effect was especially pronounced when comparing the activity of the pentaerythritol derivatives **29** and **38**, with *para*-COOH arylated Trp residues, in C2 (compound **29**) or in N1 (compound **38**) positions. Compound **29** (EC_{50} = 0.73 μM) was 3-fold more active than the prototype (EC_{50} = 2.3 μM) while **38** was devoid of antiviral activity. This data indicates that the position of the aromatic substituent is also crucial for anti-HIV activity.

Within the series of tetramers (**28–30**), the most active compound was **30** (EC_{50} = 0.07 μM), with two COOHs at positions 3 and 5 of the phenyl ring, followed by **29** (EC_{50} = 0.73 μM) and **28** (EC_{50} = 2.0 μM), with one COOH substituent in either the *para*- or *meta*- position, respectively, of the phenyl ring.

It should be emphasized that the anti-HIV-1 activity (EC_{50} = 0.07–2.4 μM) of the trimers (**21**, **22**) and tetramers (**28–30**), bearing at the C2 position of the indole ring phenyl substituents with one or two COOHs, was above that of the prototype **1** (EC_{50} = 2.3 μM) (Table 1), although their molecular weight is considerably smaller (approximately 1500 Da *versus* 3576 Da). Moreover, the activities displayed by some of these compounds (**22**, **29** and **30**) are far below their toxicity

threshold (CC_{50} > 100 μM), resulting in compounds with improved selectivity indices (CC_{50}/EC_{50} ratios, SI > 370, 137 and 1429, respectively) with respect to the prototype (SI > 43). Interestingly, tetramer **30** also shows a 330-fold improvement of activity against HIV-2 (EC_{50} = 0.02 μM) with respect to the prototype (EC_{50} = 6.6 μM).

Table 1. Anti-HIV-1 and anti-HIV-2 activity of the selected group of compounds

Compound	EC_{50}[a] (μM) HIV-1	EC_{50}[a] (μM) HIV-2	CC_{50}[b] (μM)	SI[c]	MW[d] (Da)
14	19 ± 10	>83	83 ± 4	4.4	1064.14
15	35 ± 10	>100	>100	>3	1118.12
16	41 ± 3.8	43 ± 11	>100	>2	1199.14
17	>30	>30	30 ± 4.3	ND	1300.83
18	26 ± 10	68 ± 6.0	>100	>4	1268.14
19	>9.3	>9.3	9.3 ± 0.29	ND	1154.22
20	16 ± 5.7	64 ± 28	>100	>6	1196.17
21	2.4 ± 1.3	>71	71	29.6	1196.17
22	0.27 ± 0.12	0.63 ± 0.83	>100	>370	1328.20
28	2.0 ± 0.56	0.76 ± 0.53	>100	>50	1649.66
29	0.73 ± 0.51	0.75 ± 0.83	>100	>137	1649.66
30	0.07 ± 0.04	0.02 ± 0.09	>100	>1429	1825.69
34	49	38	>100	>2	1106.24
35	43	34	>100	>2.3	1160.22
36	41	47	>100	>2.4	1238.27
38	>76	>76	76	ND	1705.76
I	>100	>100	>100	ND	835.86

II	>250	>250	>250	ND	1169.24
1	2.3 ± 0.30	6.6 ± 7.7	>100	>43	3575.84
DS-5000	0.07 ± 0.02	0.03 ± 0.01	>20	>285.7	~5000
PRM-A	3.3 ± 1.2	5.9 ± 3.7	>100	>30.3	842.80

Data are the mean ± S.D. of at least 2 to 3 independent experiments
ND: No Determined
[a] EC_{50}: 50% Effective concentration, or the concentration required to inhibit HIV-induced cytopathicity by 50%
[b] CC_{50}: 50% Cytostatic concentration, or the compound concentration required to inhibit $CD4^+$ T cell proliferation by 50%
[c] SI: Selectivity Index (CC_{50} / EC_{50})
[d] MW: Molecular weight of the molecules expressed as Da

Mode of action in the context of HIV infection

Time-of-drug-addition (TOA) experiment

To determine at which stage of the HIV replication cycle the compounds act, a time-of-drug-addition study[54,55] was performed with the most potent derivatives **22** and **30**. The HIV entry/fusion inhibitor DS5000 (DS) and the HIV reverse transcriptase inhibitor AZT were used as references. Similar to DS, HIV-1 replication, as measured by p24 antigen production, could be inhibited only if **22** and **30** were added to the cells prior to or at the moment of infection. However, addition of AZT, an inhibitor of the reverse transcription step, could be delayed up to 3 h after infection without loss of the inhibitory activity. These experiments clearly show that the compounds need to be present in T cell cultures at the start of the virus infection process (binding/adsorption period). Thus, it can be concluded that compounds **22** and **30** interfere with early event(s) of the replicative HIV cycle, very likely by inhibiting the entry of HIV into its susceptible human $CD4^+$ T cells.

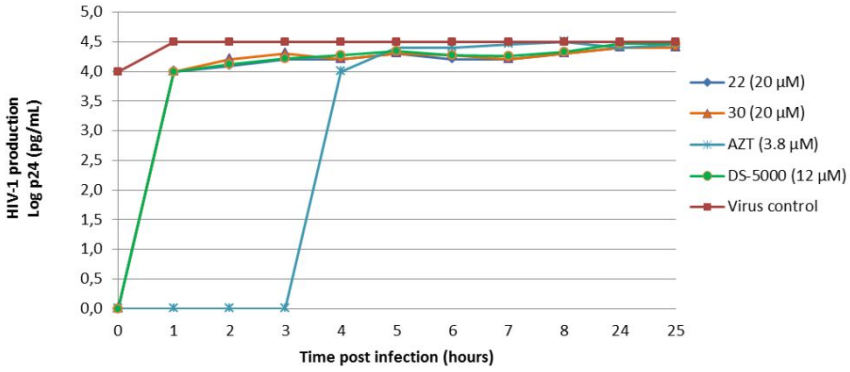

Figure 2. Results of the time-of-drug-addition experiment for compounds **22** and **30.** CD4$^+$ T cells were treated with the compounds at selected times before, during or after infection with HIV-1. 8h post-infection, cells were harvested and p24 was isolated and quantified by means of RT-qPCR. Data for DS-5000 and AZT are given as reference.

Surface plasmon resonance (SPR) analysis (HIV)

As mentioned, the prototype compound **1** inhibits an early step in the replicative cycle of HIV by interacting with the gp120 glycoprotein of the HIV envelope.[28] To investigate if this glycoprotein is also the potential target of **22** and **30,** a Surface Plasmon Resonance (SPR) experiment was carried out. First, a direct binding experiment, where gp120 was immobilized to the sensorchip, was used. Both compounds dose-dependently bound to immobilized gp120 but we could not fit the experimental data with an existing binding model, nor could steady-state affinity be measured (data not shown).

Because the sensorgrams obtained from these first direct binding experiments were inconclusive, we turned to an indirect experiment in which the inhibitory effects of **22** and **30** on the heparin-gp120 interaction, were determined. In this experiment heparin, as mimic of the host cell membrane glycosaminoglycans (GAGs), was bound to the sensorchip.[56] Both **22** and **30** were able to block the binding of gp120 onto immobilized heparin in a dose-dependent manner

(figs 3A, B). Compound **30** was the most potent inhibitor of gp120-heparin binding with an IC_{50} of 210.9 ± 30.2 nM (fig 3 C). Compound **22** was approximately 5 times less active than **30** (IC_{50} = 981.7 ± 197.0 nM), which correlates with the weaker anti-HIV-1 activity that was observed in the antiviral assay.

Overall, these data indicate that the observed *in vitro* anti-HIV activity of the Trp derivatives may be explained by their ability to specifically block the interaction between gp120 and the polysulfated polysaccharides on the host cell membranes. The tetramer **30** resulted more potent than the trimer **22.**

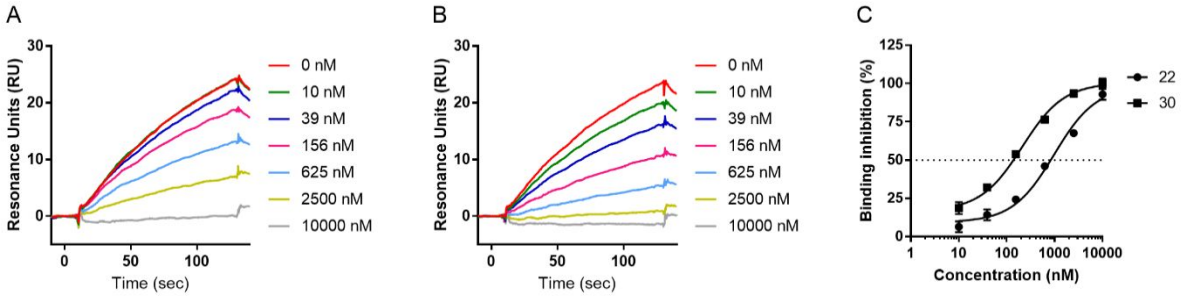

Figure 3. Inhibition of gp120-heparin binding by **22** and **30** as measured by SPR. Biotinylated heparin was captured on a Streptavidin Sensor Chip. Gp120 (10 nM) was mixed with a concentration range of compound **22** (A) or **30** (B). One representative sensorgram per compound out of three independent experiments is shown. Binding levels (RU) were converted into percentage inhibition relative to gp120 binding without compound. Mean (+SEM) and nonlinear fit of three independent experiments are shown (C).

Antiviral activity against EV71

The newly synthesized compounds were also evaluated for their *in vitro* inhibitory effects against EV-A71 (Table 2). Tryptophan prototype **1** and pirodavir, a potent EV-A71 capsid binder, were used as reference compounds.[57,58]

First, we performed an antiviral activity assay against EV-A71 BrCr, a laboratory-adapted strain, on rhabdomyosarcoma (RD) cells, which are known for their high susceptibility to EV-A71 infection.[59] For each analogue, the EC_{50} value was determined as the concentration of the drug protecting 50% of cells from EV-A71-induced cell death. Cell viability (CC_{50}) was also assessed on compound-treated, uninfected cells.

Interestingly, the SAR studies for EV-A71 revealed a similar profile to that observed for HIV. Compound **14**, bearing a phenyl ring at C2 position, and compounds **15**, **16, 17**, **18** and **19**, bearing phenyl rings substituents different than COOH (2-F, 4-NO_2, 4-Br, 4-CF_3, 4-OMe, respectively), were inactive or more than 80-fold less active than the prototype at sub-toxic concentrations. Similar to HIV, the unsubstituted tripodal and tetrapodal derivatives **I** and **II**, also proved inactive. However, the C2-arylated tryptophan derivatives **20**, **22**, **28–30**, with phenyl rings substituted with one or two COOHs were as active or even more active than the prototype **1**, indicating the importance of the carboxylic acids on the aromatic ring as a necessary requisite for antiviral activity. Notably, compound **30** resulted approximately eight-fold more potent than the prototype (EC_{50}: 0.04 μM *vs* 0.3 μM, respectively).

Interestingly, the antiviral potency of **20** (EC_{50}: 0.99 μM), bearing a COOH substituent at the *meta*-position of the phenyl ring, was 12-fold that of **21** (EC_{50}: 12.2 μM), which carried the same substituent in the *para* position. These activity data suggest that the position of the COOH substituent on the phenyl ring is crucial for antiviral activity. Furthermore, similarly to HIV, no

anti-EV-A71 activity was observed with compound **38**, possessing the aromatic substituent at N1, while the closely related analog **29** (EC_{50}: 0.37 μM), with the aromatic substituent at C2, was as active as the prototype (EC_{50}: 0.3 μM). This result clearly demonstrates that the position of the aromatic substituent also plays an important role in the anti-EV-A71 and anti-HIV activity.

Several compounds (i.e., **22, 28**, **29**) showed selectivity indices higher (SI >203, >336, 161) than those found for the prototype **1** (SI: 83) and comparable to those found for the reference compound, pirodavir (i.e., **28**: SI >336; pirodavir: SI >333). This increase in the selectivity index is particularly due to a lower cytotoxicity.

Notably, compound **30** is not toxic for the host cell. This compound turned out to have the highest selectivity index yet reported from the Trp class of compounds (SI >2500 for **30** *vs* SI: 83 for the prototype **1**).

Table 2. Antiviral activity of dendrimers against the BrCr lab strain of EV-A71 virus in RD cells.

Compound	EC_{50}[a] (μM) EV-A71	EC_{90}[b] (μM) EV-A71	CC_{50}[c] (μM)	SI[d]	MW[e] (Da)
14	>100	ND	ND	ND	1064.14
15	>89.4	ND	ND	ND	1118.12
16	28.8 ± 4.9	58.2 ± 16.3	>83.4	ND	1199.14
17	65.2	ND	ND	ND	1300.83
18	>78.9	ND	ND	ND	1268.14
19	>86.6	ND	ND	ND	1154.22
20	0.99 ± 0.01	1.35 ± 0.1	>83.6	>73.4	1196.17

21	12.2 ± 0.3	ND	>33	ND	1196.17
22	0.35 ± 0.03	0.55 ± 0.02	>75.3	>203	1328.20
28	0.19 ± 0.01	0.30 ± 0.01	>60.6	>336	1649.66
29	0.37 ± 0.08	0.63 ± 0.1	56.4	161	1649.66
30	0.04 ± 0.01	0.16 ± 0.01	>100	>2500	1825.69
38	>19.5	ND	ND	ND	1705.76
I	>120	ND	>120	ND	835.86
II	>100	ND	ND	ND	1169.24
1	0.3 ± 0.1	0.5 ± 0.06	24.9	83	3573.84
Pirodavir	0.3 ± 0.1	0.6 ± 0.2	>100	>333	369.47

All values are in micromolar (μM) and are a summary of multiple dose-response curves (>2) in multiple independent (>1) experiments.
ND: Not Determined
[a] EC_{50}: concentration of compound at which the virus-induced cytopathic effect is reduced by 50%
[b] EC_{90}: concentration of compound at which the virus-induced cytopathic effect is reduced by 90%
[c] CC_{50}: concentration of compound at which a 50% reduction in cell viability is observed
[d] SI: selectivity index (CC_{50}/EC_{50})
[e] MW: Molecular weight of the molecules expressed as Da

The compounds with the best activity/toxicity profile, **22**, **28** and **30**, were evaluated in virus-cell-based assays against a panel of clinical isolates representatives of the different (sub)genogroups of EV71 (B2, B5, C2 and C4) (Table 3). The prototype **1** was included as a reference. As previously observed for the prototype, the activity of compounds **22**, **28** and **30** on the clinical isolates was improved with respect to those found for the BrCr lab strain (sub-genogroup A). In particular, the greatest enhancement in antiviral activity was observed against sub-genogroup C4: 9-fold, 88-fold and 78-fold higher than the BrCr strain, respectively; whereas the lowest improvement was detected in the context of the infection with sub-genogroup B2 (only 2-fold, 4-fold and 6-fold improvement, respectively). It should be highlighted that the

improvement was higher for the prototype **1** than for the new compounds **22**, **28, 30** and among them for tetramers **28, 30** than for the trimer **22**.

Table 3. Evaluation of the broad-spectrum antiviral effect of compounds **22**, **28** and **30** against a representative panel of clinical EV71 isolates in RD cells.

EV71 Genogroup	Virus strain	EC_{50} (nM)[a]			
		1	**22**	**28**	**30**
A	BrCr	285 ± 70	353 ± 31	175 ± 22	109 ± 34
B2	11316	0.4 ± 0.0	179 ± 11	52 ± 1	19 ± 0.6
B5	TW/70902/08	0.2 ± 0.1	81 ± 13	18 ± 1	5.9 ± 0.7
C2	H08300 461#812	1.1 ± 0.3	57 ± 0.2	7.3 ± 0.8	2.6 ± 0.6
C4	TW/1956/05	0.2 ± 0.2	38 ± 3	2.0 ± 0.2	1.4 ± 0.7

[a]All values are in nanomolar (nM) and are obtained in multiple (>2) independent (>1) experiments.
Following microscopic quality control, at least at one concentration of compound, no virus-induced cell death was observed and the compound did not cause an adverse effect on the host cell or monolayer morphology.

Mode of action in the context of EV-A71 infection

Time-of-drug-addition (TOA) experiment (EV-A71)

To determine whether the reduced size of the newly synthetized analogues affects their mechanism of inhibition of EV-A71 replication, we performed a TOA assay with a representative member, compound **22.** In order to confirm the activity of compound **22** as an early stage inhibitor, we included the capsid binder pirodavir as a control (Figure 4).[57,60]

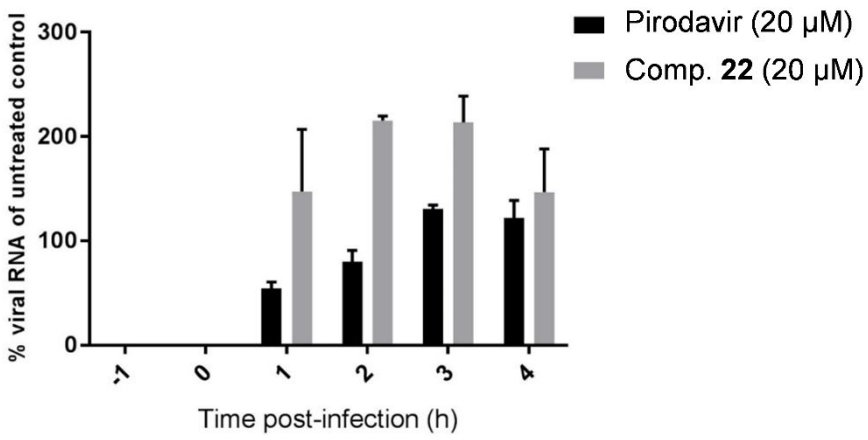

Figure 4. Time-of-drug-addition for compound **22.** RD cells were treated with the compounds at selected times before, during or after infection with EV-A71. 8h post-infection, cells were harvested and intracellular viral RNA was isolated and quantified by means of RT-qPCR.

Similar to pirodavir, only the addition of compound **22**, prior to or at the moment of infection resulted in a complete inhibition of viral replication whereas the addition after infection was associated with a complete loss of protection. This experiment clearly shows that **22**, as previously observed for prototype **1**,[29] inhibits early step(s) of the replicative cycle of EV-A71.

Cross-resistance studies

Two of the most active anti-EV-A71 compounds **22** and **30**, were also evaluated for their inhibitory activity against single mutant EV-A71 strains **VP1_S184T** and **VP1_P246S** and the double mutant **VP1_S184T_ P246S** that confer resistance to the prototype **1** (Table 4). Interestingly, **22** and **30** retain some antiviral activity (EC_{50}: 1.96-2.35 µM) against these mutant virus strains, although this activity is at least 5.6 to 6.7-fold lower than against the wild-type virus. These data point to the fact that the resistant viruses emerging under the selective pressure of **1** are also cross-resistant to **22** and **30** suggesting that these compounds are likely to share an

overall similar mechanism of antiviral activity (and resistance) and a binding site with the parent prototype **1**, namely the five-fold axis of the capsid. However, it cannot be excluded that **22** and **30**, which show some residual activity against the mutant viral strains and are the most active Trp derivatives ever reported, may give rise to additional interactions with amino acids at the five-fold axis, thus accounting for the residual activity against EV-A71 mutant viruses.

Table 4. Susceptibility of reverse-engineered EV-A71 variants to prototype **1** and compounds **22** and **30**

Virus	1 EC_{50}[a] (μM)	22 EC_{50}[a] (μM)	30 EC_{50}[a] (μM)
EV-A71 BrCr	0.28 ± 0.01	0.35 ± 0.03	0.1 ± 0.03
VP1_S184T	1.99 ± 0.10 (7.1)	2.35 ± 0.60 (6.7)	0.9 ± 0.05 (8.5)
VP1_P246S	4.71 ± 0.18 (16.8)	1.96 ± 0.04 (5.6)	0.2 ± 0.09 (1.8)
VP1_S184T_ P246S	8.93 ± 0.53 (31.9)	2.18 ± 0.08 (6.2)	0.3 ± 0.04 (3.1)

Averages and SD (standard deviation) were calculated from data obtained from three independent antiviral assays; between brackets, in red color, fold resistance.

Cryo-electron microscopy studies

To identify the binding sites of **22** and **30**, purified capsids of EV-A71 strain 11319 were incubated with each drug and vitrified for cryo-electron microscopy (cryo-EM) reconstructions. Refinement with icosahedral symmetry averaging imposed generated 2.98 Å and 2.87 Å resolution maps for **22** and **30** complexes respectively (Figure 5 and S1 Table). Sharpened maps of the two EV-A71-**22** and **30** complexes were almost identical with the map of the EV-A71 strain 11319 [42] (Figure 5A) and no extra densities on the 5-fold vertexes, where the drugs are predicted to bind, were found. However, unsharpened maps of both virus-drug complexes revealed thin extra densities covering the 5-fold axis (Fig 5B and C). This finding indicates that

the drugs bound asymmetrically on the vertex and their densities were averaged together by the imposed icosahedral symmetry, impeding the precise interpretation of the drug densities.

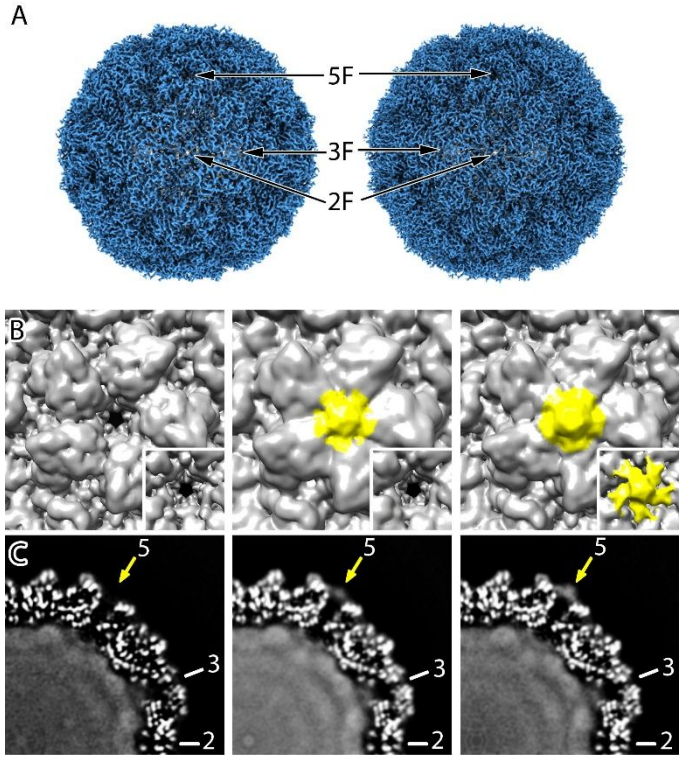

Figure 5. Cryo-EM 3D maps identified the MADAL compounds on the capsid 5-fold axis. **(A)** Surface rendering of the sharpened 3D maps for EV-A71 incubated with **22** (left) and **30** (right) showed canonical features of the capsid. Icosahedral symmetry axes were marked with arrows. **(B)** Comparison of the unsharpened maps (gray) of **22** and **30** complexes with EV-A71 showed extra densities (yellow) on the 5-fold axis. The surface rendered at 1σ and 1.9σ (insets) for EV-A71 (left), **22** (middle) and **30** (right). **(C)** Central sections of the three cryo-EM maps showed extra densities on the 5-fold-vertex covering the hole at the symmetry axis. Icosahedral symmetry axes were marked.

Compound **30** showed a stronger drug density compared to **22** (Fig 5B inlets), suggesting higher affinity of the former with respect to the latter since both compounds were incubated at the same concentration. The significant density for **30** appeared to cover the 5-fold axis like a lid and did not penetrate into the pore (Figure 5C) although it cannot be excluded the possibility that

a part of the drug might have lodged into it but its density was averaged out. The density intensity of the bound molecule in an icosahedral map is directly related to the occupancy and/or structural heterogeneity (multiple conformations) of the molecules. As shown in our previous study using prototype **1**, multiple conformations of the bound drug would decrease its density intensity.[42] This may be a common observation for drugs bound at the 5-fold axis.

Atomic models of the viral capsids were refined using the two complex maps (Figure 6A). Densities attributable to residue backbones and side chains were recognizable in the maps (Figure 6B). The capsid proteins VP1-4 did not show any significant conformational differences or rigid body movements from the atomic model of EV-A71 (RMSD 0.719 Å and 0.838 Å for **22** and **30**, respectively). Cryo-EM densities corresponding to the pocket factor were also observed in both maps (Figure 6B and data not shown). The capsid interactions with RNA genome also did not change (data not shown). Thus, binding of **22** and **30** on EV-A71 did not induce any significant conformational changes on the capsids, including pocket factor release.

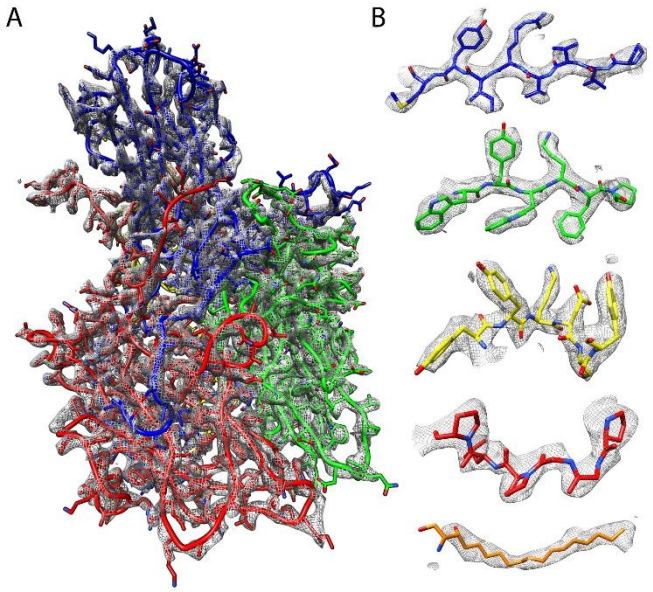

Figure 6. Atomic model built into the cryo-EM map. (A) The atomic models for EV-A71 VP1 (blue), VP2 (green), VP3 (red), VP4 (yellow), and the pocket factor (orange) were built into the cryo-EM map of the virus-**30** complex (gray mesh). **(B)** Representative residues of each VP and

the pocket-factor are shown within the corresponding cryo-EM density envelopes to illustrate the quality of the 3D map.

The superimposition of the atomic model in the unsharpened maps showed that the extra densities are strongly connected to Lys244 (K244) and Tyr245 (Y245) residues of VP1 (Figure 7A,B).

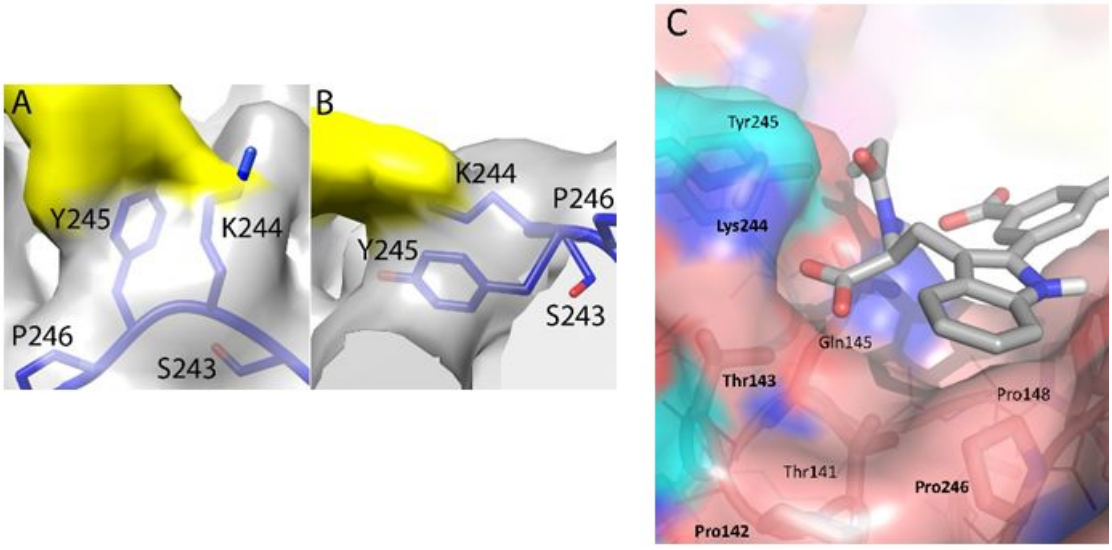

Figure 7. The drug densities are connected to two VP1 residues. (A) The icosahedrally averaged drug density (yellow, **30)** was connected mostly with Lys244 and Tyr245 on the VP1 surface (grey). The atomic model of VP1 is depicted as a blue ribbon and the side-chains are shown as sticks. The surface is rendered at 1.9σ. Neighboring residues are also labeled. **(B)** Side-view of the interaction site shows the thin drug density connected to the two VP1 residues. **(C)** Binding pose proposed by the automated docking program for the substituted Trp residue in **30** at the interface between chains E (cyan) and Q (pink) using the coordinates deposited in PDB entry 6UH7.

Further atomistic detail about the complex formed between **30** and the VP1 pentamer was gained by performing automated docking calculations with the decorated Trp moiety attached to each of its four 'legs' (Scheme 2). In the best-scored and most populated pose (Figure 7C and

Supporting Information, Figure 1) the Trp is lodged at the interface between two VP1 monomers in a cavity lined by the adjoined ^{141}TPTGQVVP^{148} and ^{242}QSKYP^{246} stretches from one subunit and the ^{242}QSKYP^{246} stretch from a neighboring subunit. In this orientation, (i) the indole ring of Trp and the phenyl ring of the isophthalate moiety stack on Pro246 and Tyr245, respectively, the latter in an edge-to-face arrangement; (ii) the Trp carboxylate establishes a hydrogen bond with the side-chain hydroxyl of Thr143 and a strong ionic interaction with the charged amino group of Lys244 from a neighboring subunit; (iii) the carboxamide nitrogen of Gln145 hydrogen bonds to one of the isophthalate carboxylates; and (iv) the other isophthalate carboxylate points to the positively charged Lys244 that is vicinal to the Tyr243 on which the phenyl ring stacks. Importantly, this pose is compatible not only with the electron density (Figure 7) but also with the fact that the ethylene linker connecting this decorated Trp to the pentaerythritol core points towards the central pore. Thus, one can figure out that one of the tetrapod's legs fits snugly into the proposed intersubunit cavity whereas the other three, which cannot bind in a similar fashion simultaneously, establish less specific van der Waals and electrostatic interactions with the residues lining the pore. Since all five VP1 subunits are identical, as are all of the dendrimer's protrusions, the overall binding mode is an average of all five combinations that is also in consonance with the average experimental electron density (Figure 8 and Supporting Information, Figure 2). Thus, it can be assumed that binding of **30** within this region prevents the interaction of the virus with its cellular (co-)receptors P-selectin glycoprotein ligand-1 (PSGL-1) and heparan sulfate thereby blocking attachment of EV-A71 to the host cells.

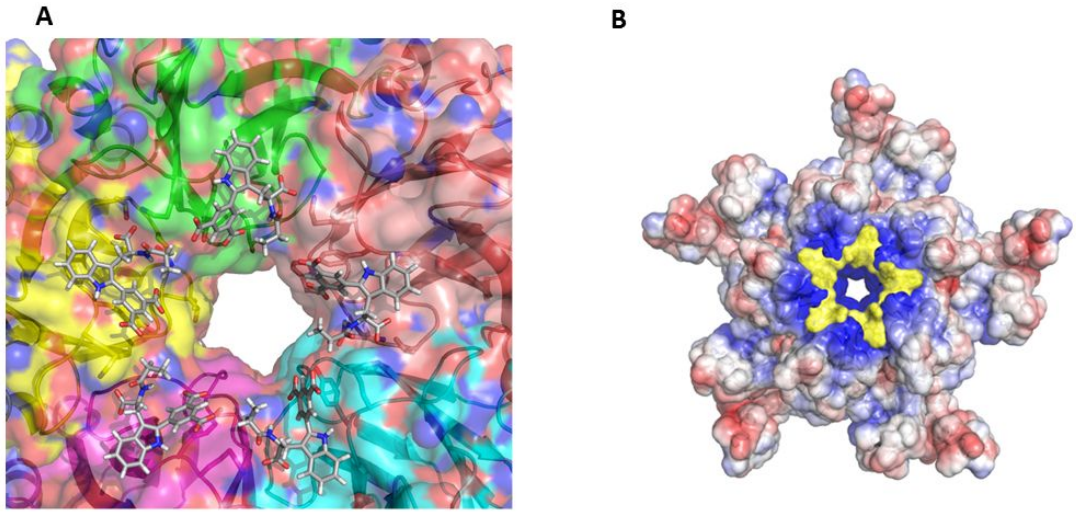

Figure 8. Proposed binding mode of the decorated Trp moiety of 30 around the 5-fold axis of the EV-A71 capsid, as deposited in PDB entry 6UH7. (A) A semitransparent surface envelops the five VP1 chains making up the pore. C atoms in chains A, E, I, M, and Q are colored in green, cyan, magenta, yellow and pink, respectively. Note that the ethylene linker points towards the central pore. **(B)** Solvent-accessible surface of the VP1 pentamer color-coded according to the molecular electrostatic potential calculated with APBS (red, -3.0 kT/e; blue, +3.0 kT/e). The yellow surface filling the subunit interfaces corresponds to the van der Waals surface of the five docked fragments shown in (**A**).

CONCLUSIONS

Using a scaffold simplification strategy, a novel generation of dual HIV and enterovirus-A71 entry inhibitors has been synthesized. These compounds contain three or four tryptophan (Trp) residues bearing at the C2 position of their indole side-chains a substituted phenyl ring. A highly efficient and scalable method has been developed for the synthesis of these compounds.

SAR studies showed that the presence of one or two carboxylates on the C2 extra phenyl rings is critical for anti-HIV and EV-A71 activity. The most potent, **22** and **30,** showed enhanced activity (~10 and 100-fold) against HIV-1 compared to the former dendrimer prototype discovered in our group. Notably, **30** is the only congener within this series that showed potent anti-HIV-2 activity. Time-of-drug-addition (TOA) experiments, followed by SPR studies

revealed that **22** and **30** act at early stages of the viral replication cycle of HIV by binding to the viral envelope glycoprotein gp120. Moreover, they also proved to be potent inhibitors of EV71, inhibiting not only the laboratory BrCr strain of EV-A71 but also clinical isolates of enteroviruses A, B and C. By means of cross-resistance studies, followed by cryo-EM, we mapped the binding region of **22** and **30** to the 5-fold axis of the EV-A71 capsid. Further details about the binding mode were provided by computer-assisted modeling studies that included docking of the common isophthaloyl-decorated Trp residue and molecular dynamics simulations. All in all, the structures presented herein provide a very consistent picture about the mode of binding of these compounds to the VP1 pentamer making up the pore region.

Compounds **22** and **30** are non-toxic for different types of host cells and show the highest selectivity indices yet reported for the Trp class of compounds. Moreover, these compounds specifically inhibit replication of HIV (HIV-1 and HIV-2) and EV71 (laboratory-adapted strain BrCr and different EV71 clinical isolates from different genogroups and geographic origins).

Taken together, these results show that this new type of Trp derivatives are important leads as dual HIV and EV71 entry inhibitors. The higher potency, lower toxicity, half-size, easy of chemical synthesis and greater opportunities for chemical optimization make them more useful than the former Trp dendrimers discovered in our group for future medicinal chemistry studies.

EXPERIMENTAL SECTION

Synthesis

General Chemistry Procedures. Commercial reagents and solvents were used as received from the suppliers without further purification unless otherwise stated. The solvents used in some reactions were dried prior to use. DMF dry was commercially available (Aldrich).

A microwave reactor Emrys™ Synthesizer (Biotage AB) was used for the reactions which needed microwave irradiation.

Analytical thin-layer chromatography (TLC) was performed on aluminum plates pre-coated with silica gel 60 (F_{254}, 0.20 mm). Products were visualized using an ultraviolet lamp (254 nm and 365 nm) or by heating after treatment with a 5% solution of phosphomolybdic acid (PMA) or vanillin in ethanol.

The compounds were purified by: a) high performance flash chromatography (HPFC) with a system "Isolera One" (Biotage) in reverse phase using water/acetonitrile (100:0 to 0:100) as eluent, b) flash column chromatography on silica gel (60 Merck 230-400 mesh), c) preparative centrifugal circular thin layer chromatography (CCTLC) on a chromatotron® (Kiesegel 60 PF254 gipshaltig, Merck) layer thickness 1 mm, flow rate 2–4 mL/min.

The purity of final compounds was at least 95% as determined by microanalyses with a Heraeus CHN-O-RAPID instrument. Analyses indicated by the symbols of the elements or functions were within ±0.4% of the theoric value.

For HPLC analysis an Agilent Technologies 1120 Compact LC with a reverse phase column ACE 5 C18-300 (4.6 mm × 150 mm, 3.5 μm) equipped with a PDA (Photo Diode Array) detector was used. Acetonitrile was used as mobile phase A, and water 0.05% of TFA was used as mobile phase B with at a flow rate of 1 $mL \cdot min^{-1}$. All retention times are quoted in minutes and the gradients are specified for each compound in the experimental data.

For high resolution mass spectrometry (HRMS) was used an Agilent 6520 Accurate Mass QTOF (quadrupole time of flight) coupled with LC/MS using an electrospray interface (ESI) working in the positive-ion (ESI^+) and negative-ion (ESI^-) mode.

NMR spectra (^{1}H, ^{13}C NMR) were recorded on a Varian UNIT INOVA-300 (300 MHz), Bruker AVANCE 300 (300 and 75 MHz), Varian INOVA-400 (400 and 100 MHz), Varian MERCURY-400 (400 and 100 MHz) and Varian-500 (500 and 125 MHz) spectrometers, using $(CD_3)_2SO$ and $CDCl_3$ as solvents. Chemical shift (δ) values are reported in parts per million (ppm) relative to tetramethylsilane (TMS) in ^{1}H and $CDCl_3$ (δ = 77.0) in ^{13}C NMR. Coupling constant (*J* values) are reported in hertz (Hz) and multiplicities of signals are indicated by the following symbol: s (singlet), d (doublet), t (triplet), q (quadruplet), m (multiplet) and bs (broad singlet). Some two-dimensional spectra (COSY, HSQC and HMBC) were performed to identify the structure.

Final compounds were lyophilized using a Telstar 6-80 system.

General coupling procedure. To a solution containing the corresponding tri- or tetrapodal polyacid (1 mmol), HATU (1.2 eq each carboxylic acid group), H-TrpOMe·HCl (1.2 eq each carboxylic acid group) or C2-isophthtaloyl N^{α}-CBz-tryptophan methyl ester (1.2 eq each carboxylic acid group) in DMF (20 mL), DIPEA (3.4 eq each carboxylic acid group) was added. The reaction mixture was stirred at 30 ºC for 48 h and then evaporated to dryness. The residue was dissolved in dichloromethane (20 mL) and washed successively with aqueous solutions of citric acid (10%) (3 x 20 mL), saturated $NaHCO_3$ (3 x 20 mL), and brine (3 x 20 mL). The organic phase was dried over anhydrous Na_2SO_4, filtered and evaporated to dryness. The residue was purified on a Biotage HPFC (High Performance Flash Chromatography) purification system on reverse phase using water/acetonitrile (100:0 to 0:100) as eluent to give the corresponding compound.

General procedure for C2 arylation of indole. The corresponding Trp trimer or tetramer (1 mmol), aryl iodide (2 eq for each Trp), $AgBF_4$ (2 eq for each Trp), TFA (1 eq for each Trp) and $Pd(OAc)_2$ (5% mol) were placed in a microwave reactor vessel in dry DMF (2 mL). The mixture was heated under microwave irradiation (250 W) at 120 ºC for 30 min. The resulting suspension was filtered through Whatman® filter paper 42, and the solvent was removed under vacuum. The residue was dissolved in ethyl acetate (20 mL) and washed successively with saturated $NaHCO_3$ (3 x 20 mL), and brine (3 x 20 mL). The organic phase was dried over anhydrous Na_2SO_4, filtered and evaporated to dryness. The residue was purified by CCTLC using dichloromethane/methanol (20:1) as eluent.

General procedure for N1 benzylation of indole. To a solution containing the corresponding Trp trimer or tetramer (1.0 mmol) in dry acetonitrile (10 mL), Cs_2CO_3 (1.5 eq for each Trp) was added and the mixture was stirred at room temperature for 15 minutes. Then the corresponding benzyl bromide (1.2 eq for each Trp) was added and the reaction mixture was stirred at 80 ºC for 6 h. The mixture was evaporated to dryness, dissolved in dichloromethane (20 mL) and washed successively with citric acid (3 x 20 mL) and brine (3 x 20 mL). The organic phase was dried over anhydrous Na_2SO_4 and evaporated to dryness. The residue was purified on a Biotage HPFC (High Performance Flash Chromatography) purification system on reverse phase using water/acetonitrile (100:0 to 0:100) as eluent.

General procedure for methyl ester deprotection. To a solution containing the corresponding methyl ester derivative (1.0 mmol) in THF (10 mL) at 0 ºC (ice-bath), a solution of $LiOH{\cdot}H_2O$ (2 eq for each methyl ester group) in water (2 mL) was added, and the mixture was stirred at room temperature overnight. Then 1 N hydrochloric acid aqueous solution was added to reach pH = 2, and volatiles were evaporated to dryness. The residue was dissolved in ethyl

acetate (15 mL) and washed with H_2O (3 x 10 mL). The organic phase was dried over anhydrous Na_2SO_4, filtered and evaporated to dryness. The compounds were precipitated with diethyl ether to afford the pure deprotected derivatives.

Trimer 4. Following the general coupling procedure, compound **3**[48] (500 mg, 1.80 mmol), HATU (2.47 g, 6.49 mmol), H-TrpOMe·HCl (1.65 mg, 6.49 mmol,) and DIPEA (3.14 mL, 18.03 mmol) afforded 1.53 g (97%) of **4** as an amorphous solid of cream color. ^{1}H NMR (400 MHz, $CDCl_3$) δ: 8.59 (d, J = 6.3 Hz, 3H, NH-1^{i}Trp), 7.43 (d, J = 7.9 Hz, 3H, Ar), 7.27–7.24 (m, 3H, Ar), 7.11 (ddt, J = 8.0, 7.0, 0.9 Hz, 3H, Ar), 7.03 (ddt, J = 7.9, 7.0, 1.0 Hz, 3H, Ar), 6.87 (d, J = 2.3 Hz, 3H, Ar), 6.40 (t, J = 8.1 Hz, 3H, NHCO), 4.87–4.80 (m, 3H, α-CHTrp), 3.27 (dd, J = 14.9, 5.1 Hz, 3H, β-CH_2Trp), 3.15 (dd, J = 14.9, 6.8 Hz, 3H, β-CH_2Trp), 1.92–1.70 (m, 12H, CH_2). HPLC [gradient: A:B, 10-100% of A in 10 min]: 6.865 min. HRMS (ESI$^+$) m/z: Cald for $C_{46}H_{51}N_7O_{11}$ 877.3177; found 877.3163.

Trimer 5. Following the general C2 arylation, procedure, compound **4** (50 mg, 0.057 mmol), iodobenzene (38.3 µL, 0.342 mmol), $Pd(OAc)_2$ (0.6 mg, 0.003 mmol,), $AgBF_4$ (66.5 mg, 0.342 mmol) and TFA (13.1 µL, 0.171 mmol) afforded 35.9 mg (56.9%) of **5** as an amorphous solid of cream color. ^{1}H NMR (500 MHz, $CDCl_3$) δ: 8.45 (bs, 3H, NH-1^{i}Trp), 7.53–7.48 (m, 9H, Ar), 7.41 (t, J = 7.6 Hz, 6H, Ar), 7.35–7.30 (m, 3H, Ar), 7.25 (d, J = 2.9 Hz, 3H, Ar), 7.16–7.11 (m, 3H, Ar), 7.10–7.05 (m, 3H, Ar), 5.81 (d, J = 7.9 Hz, 3H, NHCO), 4.79–4.74 (m, 3H, α-CHTrp), 3.51 (dd, J = 14.7, 5.7 Hz, 3H, β-CH_2Trp), 3.44 (dd, J = 14.8, 6.0 Hz, 3H, β-CH_2Trp), 3.37 (s, 9H, OCH_3), 1.74–1.62 (m, 6H, CH_2), 1.57–1.49 (m, 3H, CH_2), 1.43–1.33 (m, 3H, CH_2). HPLC [gradient: A:B, 10-100% of A in 10 min]: 4.999 min. HRMS (ESI$^+$) m/z: Cald for $C_{64}H_{63}N_7O_{11}$ 1105.4116; found 1105.4102.

Trimer 6. Following the general C2 arylation procedure, compound **4** (100 mg, 0.114 mmol), 2-fluoroiodobenzene (79 μL, 0.683 mmol), $Pd(OAc)_2$ (1.3 mg, 0.006 mmol,), $AgBF_4$ (132.97 mg, 0.683 mmol) and TFA (26 μL, 0.342 mmol) afforded 38.2 mg (29%) of **6** as an amorphous solid of cream color. ^{1}H NMR (300 MHz, $CDCl_3$) δ: 8.45 (bs, 3H, NH-1^{i}Trp), 7.58–7.47 (m, 6H, Ar), 7.42–7.34 (m, 3H, Ar), 7.30–7.06 (m, 15H, Ar), 5.87 (d, J = 7.9 Hz, 3H, NHCO), 4.84–4.75 (m, 3H, α-CHTrp), 3.51–3.31 (m, 15H, β-CH_2Trp and OCH_3), 1.82–1.60 (m, 9H, CH_2), 1.56–1.42 (m, 3H, CH_2). HPLC [gradient: A:B, 10-100% of A in 10 min]: 7.406 min. HRMS (ESI$^+$) m/z: Cald for $C_{64}H_{60}F_3N_7O_{11}$ 1159.3833; found 1159.3829.

Trimer 7. Following the general C2 arylation procedure, compound **4** (50 mg, 0.057 mmol), 1-iodo-4-nitrobenzene (85.2 mg, 0.342 mmol), $Pd(OAc)_2$ (0.6 mg, 0.003 mmol,), $AgBF_4$ (66.6 mg, 0.342 mmol) and TFA (13 μL, 0.171 mmol) afforded 33.4 mg (47%) of **7** as an amorphous solid of cream color. ^{1}H NMR (300 MHz, DMSO) δ: 11.51 (bs, 3H, NH-1^{i}Trp), 8.48 (d, J = 7.7 Hz, 3H, NHCO), 8.37–8.26 (m, 6H, Ar), 7.96–7.83 (m, 6H, Ar), 7.59 (d, J = 7.9 Hz, 3H, Ar), 7.40–7.32 (m, 3H, Ar), 7.14 (t, J = 7.6 Hz, 3H, Ar), 7.02 (t, J = 7.4 Hz, 3H, Ar), 4.59–4.56 (m, 3H, α-CHTrp), 3.52–3.20 (m, 15H, OCH_3 and β-CH_2Trp), 1.97–1.72 (m, 12H, CH_2). HPLC [gradient: A:B, 10-100% of A in 10 min]: 6.825 min. HRMS (ESI$^+$) m/z: Cald for $C_{64}H_{60}N_{10}O_{17}$ 1240.3668; found 1240.3657.

Trimer 8. Following the general C2 arylation procedure, compound **4** (100 mg, 0.114 mmol), 1-bromo-4-iodobenzene (193 mg, 0.683 mmol), $Pd(OAc)_2$ (1.3 mg, 0.006 mmol,), $AgBF_4$ (132.97 mg, 0.683 mmol) and TFA (26 μL, 0.342 mmol) afforded 57.3 mg (37%) of **8** as an amorphous solid of cream color. ^{1}H NMR (300 MHz, $CDCl_3$) δ: 8.51–8.44 (m, 3H, NH-1^{i}Trp), 7.61–7.47 (m, 9H, Ar), 7.40 (d, J = 8.0 Hz, 6H, Ar), 7.30–7.23 (m, 3H, Ar), 7.16 (t, J = 7.2 Hz, 3H, Ar), 7.08 (t, J = 7.4 Hz, 3H, Ar), 5.95 (d, J = 7.9 Hz, 3H, NHCO), 4.83–4.74 (m, 3H, α-

CHTrp), 3.52–3.31 (m, 15H, OCH_3 and β-CH_2Trp), 1.81–1.40 (m, 12H, CH_2). HPLC [gradient: A:B, 10-100% of A in 10 min]: 8.590 min. HRMS (ESI^+) m/z: Cald for $C_{64}H_{60}Br_3N_7O_{11}$ 1339.7731; found 1339.7728.

Trimer 9. Following the general C2 arylation procedure, compound **4** (100 mg, 0.114 mmol), 4-iodobenzotrifluoride (186 mg, 0.683 mmol), $Pd(OAc)_2$ (1.3 mg, 0.006 mmol,), $AgBF_4$ (132.97 mg, 0.683 mmol) and TFA (26 μL, 0.342 mmol) afforded 48.6 mg (33%) of **9** as an amorphous solid of cream color. ^1H NMR (300 MHz, $CDCl_3$) δ: 8.47 (bs, 3H, NH-1^{i}Trp), 7.82 (s, 3H, Ar), 7.76 (d, J = 7.4 Hz, 3H, Ar), 7.66–7.50 (m, 9H, Ar), 7.31–7.25 (m, 3H, Ar), 7.20–7.06 (m, 6H, Ar), 5.97 (d, J = 8.1 Hz, 3H, NHCO), 4.83–4.74 (m, 3H, α-CHTrp), 3.54–3.31 (m, 15H, OCH_3 and β-CH_2Trp), 1.80–1.42 (m, 12H, CH_2). HPLC [gradient: A:B, 10-100% of A in 10 min]: 8.741 min. HRMS (ESI^+) m/z: Cald for $C_{67}H_{60}F_9N_7O_{11}$ 1309.3738; found 1309.3759.

Trimer 10. Following the general C2 arylation procedure, compound **4** (100 mg, 0.114 mmol), 4-iodoanisole (159.9 mg, 0.683 mmol), $Pd(OAc)_2$ (1.3 mg, 0.006 mmol,), $AgBF_4$ (132.97 mg, 0.683 mmol) and TFA (26 μL, 0.342 mmol) afforded 51.4 mg (38%) of **10** as an amorphous solid of cream color. ^1H NMR (300 MHz, $CDCl_3$) δ: 8.36 (bs, 3H, NH-1^{i}Trp), 7.52–7.42 (m, 9H, Ar), 7.28–7.23 (m, 3H, Ar), 7.17–7.03 (m, 6H, Ar), 7.01–6.93 (m, 6H, Ar), 5.87 (d, J = 7.9 Hz, 3H, NHCO), 4.82–4.72 (m, 3H, α-CHTrp), 3.85–3.76 (m, 9H, OCH_3), 3.53–3.35 (m, 15H, OCH_3 and β-CH_2Trp), 1.83–1.40 (m, 12H, CH_2). HPLC [gradient: A:B, 10-100% of A in 10 min]: 7.447 min. HRMS (ESI^+) m/z: Cald for $C_{67}H_{69}N_7O_{14}$ 1195.4433; found 1195.4447.

Trimer 11. Following the general C2 arylation procedure, compound **4** (100 mg, 0.114 mmol), methyl 3-iodobenzoate (179.1 mg, 0.683 mmol), $Pd(OAc)_2$ (1.3 mg, 0.006 mmol,), $AgBF_4$ (132.97 mg, 0.683 mmol) and TFA (26 μL, 0.342 mmol) afforded 56 mg (38%) of **11** as an amorphous solid of cream color. ^1H NMR (300 MHz, $CDCl_3$) δ: 8.58 (s, 3H, NH-1^{i}Trp), 8.24–

8.20 (m, 3H, Ar), 8.01 (dt, J = 7.8, 1.4 Hz, 3H, Ar), 7.77 (dt, J = 7.9 Hz, 1.5 Hz, 3H, Ar), 7.56–7.48 (m, 6H, Ar), 7.31–7.27 (m, 3H, Ar), 7.19–7.05 (m, 6H, Ar), 6.01 (d, J = 8.1 Hz, 3H, NHCO), 4.84–4.74 (m, 3H, α-CHTrp), 3.90 (s, 9H, OCH_3), 3.55–3.33 (m, 15H, OCH_3 and β-CH_2Trp), 1.82–1.42 (m, 12H, CH_2). HPLC [gradient: A:B, 10-100% of A in 10 min]: 6.026 min. HRMS (ESI^+) m/z: Cald for $C_{70}H_{69}N_7O_{17}$ 1279.3811; found 1279.3808.

Trimer 12. Following the general C2 arylation procedure, compound **4** (100 mg, 0.114 mmol), methyl 4-iodobenzoate (179.2 mg, 0.684 mmol), $Pd(OAc)_2$ (1.3 mg, 0.006 mmol,), $AgBF_4$ (132.97 mg, 0.683 mmol) and TFA (26 µL, 0.342 mmol) afforded 54.1 mg (37%) of **12** as an amorphous solid of cream color. ^1H NMR (400 MHz, $CDCl_3$) δ: 8.73 (s, 3H. NH-1^{i}Trp), 8.06 (d, J = 8.5 Hz, 6H, Ar), 7.62 (d, J = 8.5 Hz, 6H, Ar), 7.52 (d, J = 7.9 Hz, 3H, Ar), 7.32–7.27 (m, 3H, Ar), 7.18–7.12 (m, 3H, Ar), 7.10–7.04 (m, 3H, Ar), 6.07 (d, J = 8.0 Hz, 3H, NHCO), 4.83–4.76 (m, 3H, α-CHTrp), 3.89 (s, 9H, OCH_3), 3.52 (dd, J = 14.7, 6.2 Hz, 3H, β-CH_2Trp), 3.46–3.40 (m, 3H, β-CH_2Trp), 3.39 (s, 9H, OCH_3), 1.73–1.57 (m, 8H, CH_2), 1.51–1.41 (m, 4H, CH_2). HPLC [gradient: A:B, 10-100% of A in 10 min]: 6.222 min. HRMS (ESI^+) m/z: Cald for $C_{70}H_{69}N_7O_{17}$ 1279.3811; found 1279.3808.

Trimer 13. Following the general C2 arylation procedure, compound **4** (100 mg, 0.114 mmol), dimethyl 5-iodoisophthalate (218 mg, 0.684 mmol), $Pd(OAc)_2$ (1.3 mg, 0.006 mmol,), $AgBF_4$ (132.97 mg, 0.683 mmol) and TFA (26 µL, 0.342 mmol) afforded 57.3 mg (35%) of **13** as an amorphous solid of cream color. ^1H NMR (300 MHz, $CDCl_3$) δ: 8.89 (bs, 3H, NH-1^{i}Trp), 8.56 (bs, 3H, Ar), 8.38 (d, J = 1.6 Hz, 6H, Ar), 7.54 (d, J = 7.8 Hz, 3H, Ar), 7.30–7.24 (m, 3H, Ar), 7.19–7.03 (m, 6H, Ar), 6.19 (d, J = 8.2 Hz, 3H, NHCO), 4.84–4.74 (m, 3H, α-CHTrp), 3.90 (s, 18H, OCH_3), 3.51–3.29 (m, 15H, OCH_3 and β-CH_2Trp), 1.78–1.47 (m, 12H, CH_2). HPLC

[gradient: A:B, 10-100% of A in 10 min]: 7.239 min. HRMS (ESI^+) m/z: Cald for $C_{76}H_{75}N_7O_{23}$ 1453.3506; found 1453.3498.

Trimer 14. Following the general procedure for methyl ester deprotection, compound **5** (60 mg, 0.0542 mmol) gave 57 mg (quant) of **14** as an amorphous white solid. ^1H NMR (400 MHz, DMSO-d_6) δ: 11.16 (s, 3H, NH-1^{i}Trp), 8.27 (d, J = 8.2 Hz, 3H, NHCO), 7.62 (d, J = 7.7 Hz, 9H, Ar), 7.44 (t, J = 7.6 Hz, 6H, Ar), 7.36–7.26 (m, 6H, Ar), 7.04 (t, J = 7.5 Hz, 3H, Ar), 6.96 (t, J = 7.4 Hz, 3H, Ar), 4.57–4.49 (m, 3H, α-CHTrp), 3.30 (dd, J = 14.4, 6.7 Hz, 3H, β-CH_2Trp), 3.12 (dd, J = 14.4, 7.7 Hz, 3H, β-CH_2Trp), 1.88–1.70 (m, 12H. CH_2). ^{13}C NMR (100 MHz, DMSO-d_6) δ: 174.0, 171.0, 136.5, 135.9, 133.5, 129.6, 129.3, 128.6, 128.1, 122.1, 119.62, 119.4, 111.7, 108.2, 93.6, 53.8, 31.2, 29.9, 28.0. HPLC [gradient: A:B, 10-100% of A in 10 min]: 5.150 min. HRMS (ESI^-) m/z: Cald for $C_{61}H_{57}N_7O_{11}$: 1063.4116; found 1063.4102. Anal. Cal. for $C_{61}H_{57}N_7O_{11}$ C, 68.85; H, 5.40. Found: C, 68.64; H, 5.20.

Trimer 15. Following the general procedure for methyl ester deprotection, compound **6** (58 mg, 0.05 mmol) gave 55 mg (quant) of **15** as an amorphous white solid. ^1H NMR (400 MHz, DMSO-d_6) δ: 11.24 (s, 3H, NH-1^{i}Trp), 8.18 (d, J = 8.1 Hz, 3H, NHCO), 7.71 (d, J = 7.9 Hz, 3H, Ar), 7.62–7.56 (m, 3H, Ar), 7.53–7.46 (m, 3H, Ar), 7.42–7.32 (m, 9H, Ar), 7.15 (t, J = 7.5 Hz, 3H, Ar), 7.07 (t, J = 7.4 Hz, 3H, Ar), 4.54–4.46 (m, 3H, α-CHTrp), 3.22 (dd, J = 14.4, 6.6 Hz, 3H, β-CH_2Trp), 3.11 (dd, J = 14.4, 7.5 Hz, 3H, β-CH_2Trp), 1.95–1.77 (m, 12H, CH_2). ^{13}C NMR (100 MHz, DMSO-d_6) δ: 173.6, 170.6, 161.0, 158.5, 136.5, 132.4, 132.4, 130.6, 130.6, 130.1, 128.4, 125.4, 124.9, 124.9, 122.0, 121.1, 121.0, 119.4, 119.2, 116.5, 116.3, 111.6, 109.6, 93.3, 53.4, 34.9, 31.0, 30.9, 29.6, 29.5, 27.6. HPLC [gradient: A:B, 10-100% of A in 10 min]: 6.131 min. HRMS (ESI^-) m/z: Cald for $C_{61}H_{54}F_3N_7O_{11}$: 1117.3833; found 1117.3828. Anal. Cal. for $C_{61}H_{54}F_3N_7O_{11}$: C, 65.53; H, 4.87. Found: C, 65.28; H, 4.69.

Trimer 16. Following the general procedure for methyl ester deprotection, compound **7** (53 mg, 0.043 mmol) gave 51 mg (quant) of **16** as an amorphous white solid. ^{1}H NMR (400 MHz, DMSO-d_6) δ: 11.48 (s, 3H, NH-1^{i}Trp), 8.36–8.39 (m, 9H, NHCO and Ar), 7.94 (d, J = 8.8 Hz, 6H, Ar), 7.70 (d, J = 8.0 Hz, 3H, Ar), 7.38 (d, J = 8.1 Hz, 3H, Ar), 7.14 (t, J = 7.5 Hz, 3H, Ar), 7.03 (t, J = 7.4 Hz, 3H, Ar), 4.61–4.53 (m, 3H, α-CHTrp), 3.40 (dd, J = 14.6, 6.8 Hz, 3H, β-CH_2Trp), 3.24 (dd, J = 14.5, 7.7 Hz, 3H, β-CH_2Trp), 1.94–1.71 (m, 12H, CH_2). ^{13}C NMR (100 MHz, DMSO-d_6) δ: 173.5, 170.9, 146.4, 139.8, 139.6, 137.0, 133.2, 129.3, 128.9, 125.4, 124.3, 123.2, 119.9, 119.7, 111.9, 111.1, 93.4, 53.4, 34.9, 30.9, 29.7, 29.7, 29.5, 27.8. HPLC [gradient: A:B, 10-100% of A in 10 min]: 6.456 min. HRMS (ESI$^-$) m/z: Cald for $C_{61}H_{54}N_{10}O_{17}$ 1198.3668; found 1198.3655. Anal. Cal. for $C_{61}H_{54}N_{10}O_{17}$: C, 61.10; H, 4.54. Found: C, 61.03; H, 4.39.

Trimer 17. Following the general procedure for methyl ester deprotection, compound **8** (61 mg, 0.045 mmol) gave 59 mg (quant) of **17** as an amorphous white solid. ^{1}H NMR (400 MHz, DMSO-d_6) δ: 11.24 (s, 3H, NH-1^{i}Trp), 8.30 (d, J = 8.2 Hz, 3H, NHCO), 7.70–7.64 (m, 9H, Ar), 7.63–7.59 (m, 6H, Ar), 7.34 (d, J = 8.0 Hz, 3H, Ar), 7.09 (t, J = 7.5 Hz, 3H, Ar), 7.00 (t, J = 7.5 Hz, 3H, Ar), 4.59–4.52 (m, 3H, α-CHTrp), 3.31 (dd, J = 14.5, 6.9 Hz, 3H, β-CH_2Trp), 3.19–3.10 (m, 3H, β-CH_2Trp), 1.95–1.74 (m, 12H, CH_2). ^{13}C NMR (100 MHz, DMSO-d_6) δ: 173.6, 170.8, 139.6, 136.4, 134.4, 132.5, 132.0, 130.4, 129.3, 128.5, 125.4, 122.2, 121.1, 119.51, 119.4, 111.6, 108.6, 93.4, 53.5, 49.1, 34.9, 31.0, 30.9, 29.8, 29.7, 27.8, 21.5. HPLC [gradient: A:B, 10-100% of A in 10 min]: 7.242 min. HRMS (ESI$^-$) m/z: Cald for $C_{61}H_{54}Br_3N_7O_{11}$ 1297.1431; found 1297.1388. Anal. Cal. for $C_{61}H_{54}Br_3N_7O_{11}$: C, 56.32; H, 4.18. Found: C, 56.20; H, 4.03.

Trimer 18. Following the general procedure for methyl ester deprotection, compound **9** (57.2 mg, 0.044 mmol) gave 55 mg (quant) of **18** as an amorphous white solid. ^{1}H NMR (400 MHz, DMSO-d_6) δ: 11.38 (s, 3H, NH-1^{i}Trp), 8.34 (d, J = 8.3 Hz, 3H, NHCO), 8.01–7.94 (m, 6H, Ar),

7.74–7.67 (m, 9H, Ar), 7.36 (d, J = 8.1 Hz, 3H, Ar), 7.11 (t, J = 7.5 Hz, 3H, Ar), 7.02 (t, J = 7.5 Hz, 3H, Ar), 4.61–4.54 (m, 3H, α-CHTrp), 3.35 (dd, J = 14.5, 6.8 Hz, 3H, β-CH_2Trp), 3.18 (dd, J = 14.5, 7.5 Hz, 3H, β-CH_2Trp), 1.93–1.73 (m, 12H, CH_2). ^{13}C NMR (100 MHz, DMSO-d_6) δ: 173.6, 170.8, 162.8, 139.6, 136.5, 134.2, 133.8, 132.2, 130.5, 130.2, 129.9, 129.5, 129.2, 128.7, 126.0, 125.4, 124.7, 124.6, 124.3, 124.3, 123.3, 122.5, 120.6, 119.7, 119.5, 111.7, 109.3, 93.4, 53.5, 36.2, 34.9, 31.2, 30.9, 29.7, 28.2, 27.8. HPLC [gradient: A:B, 10-100% of A in 10 min]: 7.619 min. HRMS (ESI$^-$) m/z: Cald for $C_{64}H_{54}F_9N_7O_{11}$ 1267.3738; found 1267.3761. Anal. Cal. for $C_{64}H_{54}F_9N_7O_{11}$: C, 60.62; H, 4.29. Found: C, 60.43; H, 4.13.

Trimer 19. Following the general procedure for methyl ester deprotection compound **10** (50 mg, 0.04 mmol) gave 46 mg (quant) of **19** as an amorphous white solid. ^{1}H NMR (400 MHz, DMSO-d_6) δ: 11.13 (s, 3H, NH-1^{i}Trp), 8.33 (d, J = 8.3 Hz, 3H, NHCO), 7.68 (d, J = 7.9 Hz, 3H, Ar), 7.64 (d, J = 8.5 Hz, 6H, Ar), 7.36 (d, J = 7.9 Hz, 3H, Ar), 7.14–7.06 (m, 9H, Ar), 7.03 (t, J = 7.4 Hz, 3H, Ar), 4.65–4.57 (m, 3H, α-CHTrp), 3.85 (s, 9H, OCH_3), 3.41–3.30 (m, 3H, β-CH_2Trp), 3.16 (dd, J = 14.4, 7.6 Hz, 3H, β-CH_2Trp), 2.03–1.82 (m, 12H, CH_2). ^{13}C NMR (100 MHz, DMSO-d_6) δ: 173.8, 170.8, 159.1, 136.1, 135.7, 129.7, 129.5, 125.7, 121.5, 119.2, 119.1, 114.6, 111.3, 107.1, 93.4, 55.6, 53.6, 31.2, 31.0, 30.9, 29.8, 29.7, 27.9. HPLC [gradient: A:B, 10-100% of A in 10 min]: 5.999 min. HRMS (ESI$^-$) m/z: Cald for $C_{64}H_{63}N_7O_{14}$ 1153.4433; found 1153.4458. Anal. Cal. for $C_{64}H_{63}N_7O_{14}$: C, 66.60; H, 5.50. Found: C, 66.40; H, 5.28.

Trimer 20. Following the general procedure for methyl ester deprotection, compound **11** (52 mg, 0.04 mmol) gave 49.2 mg (quant) of **20** as an amorphous white solid. ^{1}H NMR (400 MHz, DMSO-d_6) δ: 11.31 (s, 3H, NH-1^{i}Trp), 8.30 (d, J = 8.2 Hz, 3H, NHCO), 8.18 (bs, 3H, Ar), 7.92 (d, J = 7.7 Hz, 3H, Ar), 7.88 (d, J = 8.1 Hz, 3H, Ar), 7.64 (d, J = 7.9 Hz, 3H, Ar), 7.58 (t, J = 7.7 Hz, 3H, Ar), 7.32 (d, J = 8.0 Hz, 3H, Ar), 7.07 (t, J = 7.5 Hz, 3H, Ar), 6.98 (t, J = 7.4 Hz, 3H,

Ar), 4.56–4.48 (m, 3H, α-CHTrp), 3.32 (dd, J = 14.4, 7.2 Hz, 3H, β-CH_2Trp), 3.14 (dd, J = 14.4, 7.4 Hz, 3H, β-CH_2Trp), 1.93–1.70 (m, 12H, CH_2). ^{13}C NMR (100 MHz, DMSO-d_6) δ: 173.6, 170.8, 167.7, 136.5, 134.7, 133.6, 132.6, 131.9, 129.4, 129.3, 129.2, 128.6, 122.2, 119.5, 119.4, 111.6, 108.5, 93.4, 53.6, 31.0, 29.7, 27.7. HPLC [gradient: A:B, 10-100% of A in 10 min]: 4.738 min. HRMS (ESI$^-$) m/z: Cald for $C_{64}H_{57}N_7O_{17}$ 1195.3811; found 1195.3810. Anal. Cal. for $C_{64}H_{57}N_7O_{17}$: C, 64.26; H, 4.80. Found: C, 63.98; H, 4.20.

Trimer 21. Following the general procedure for methyl ester deprotection, compound **12** (73.7 mg, 0.057 mmol) gave 68 mg (quant) of **21** as an amorphous white solid. ^{1}H NMR (400 MHz, DMSO-d_6) δ: 11.31 (s, 3H, NH-1^{i}Trp), 8.34 (d, J = 8.2 Hz, 3H, NHCO), 8.02 (d, J = 8.2 Hz, 6H, Ar), 7.78 (d, J = 8.3 Hz, 6H, Ar), 7.66 (d, J = 8.0 Hz, 3H, Ar), 7.33 (d, J = 8.1 Hz, 3H, Ar), 7.08 (t, J = 7.3 Hz, 3H, Ar), 6.98 (t, J = 7.5 Hz, 3H, Ar), 4.59–4.51 (m, 3H, α-CHTrp), 3.34 (dd, J = 14.4, 7.0 Hz, 3H, β-CH_2Trp), 3.16 (dd, J = 14.4, 7.6 Hz, 3H, β-CH_2Trp), 1.93–1.73 (m, 12H, CH_2). ^{13}C NMR (100 MHz, DMSO-d_6) δ: 173.6, 170.8, 167.5, 137.4, 136.6, 134.3, 130.06, 129.6, 129.3, 128.2, 122.5, 119.7, 119.4, 111.7, 109.6, 93.3, 53.5, 30.9, 30.9, 29.7, 27.9. HPLC [gradient: A:B, 10-100% of A in 10 min]: 4.651 min. HRMS (ESI$^-$) m/z: Cald for $C_{64}H_{57}N_7O_{17}$ 1195.3811; found 1195.3806. Anal. Cal. for $C_{64}H_{57}N_7O_{17}$: C, 64.26; H, 4.80. Found: C, 64.04; H, 4.60.

Trimer 22. Following the general procedure for methyl ester deprotection, compound **13** (35.1 mg, 0.024 mmol) gave 32 mg (quant) of **22** as an amorphous white solid. ^{1}H NMR (400 MHz, DMSO-d_6) δ: 11.43 (s, 3H, NH-1^{i}Trp), 8.44 (m, 3H, Ar), 8.39–8.36 (m, 6H, Ar), 8.31 (d, J = 8.0 Hz, 3H, NHCO), 7.65 (d, J = 8.0 Hz, 3H, Ar), 7.34 (d, J = 8.1 Hz, 3H, Ar), 7.13–7.06 (m, 3H, Ar), 7.02–6.96 (m, 3H, Ar), 4.53–4.46 (m, 3H, α-CHTrp), 3.35 (dd, J = 14.4, 7.8 Hz, 3H, β-CH_2Trp), 3.17 (dd, J = 14.4, 7.0 Hz, 3H, β-CH_2Trp), 1.97–1.69 (m, 12H, CH_2). ^{13}C NMR (100

MHz, DMSO-d_6) δ: 173.3, 170.8, 167.0, 136.6, 134.2, 133.9, 133.0, 132.3, 129.2, 129.0, 122.4, 119.6, 119.5, 111.7, 109.0, 93.3, 53.4, 30.9, 30.9, 29.7, 27.5. HPLC [gradient: A:B, 10-100% of A in 10 min]: 3.815 min. HRMS (ESI^-) m/z: Cald for $C_{67}H_{57}N_7O_{23}$ 1327.3506; found 1327.3498. Anal. Cal. for $C_{67}H_{57}N_7O_{23}$: C, 60.59; H, 4.33. Found: C, 60.03; H, 4.01.

Tetramer 24. Following the general coupling procedure, compound **23**[49,50] (200 mg, 0.47 mmol), HATU (0.85 g, 2.26 mmol), H-TrpOMe·HCl (0.55 mg, 2.26 mmol,), DIPEA (0.82 mL, 4.71 mmol) afforded 470 mg (82%) of **24** as an amorphous solid of cream color. ^{1}H NMR (300 MHz, $CDCl_3$) δ: 9.29 (d, J = 2.4 Hz, 4H, NH-1^{i}Trp), 7.48 (dd, J = 6.9, 1.9 Hz, 4H, Ar), 7.25–7.19 (m, 4H, Ar), 7.13–7.01 (m, 8H, Ar), 6.96 (d, J = 2.3 Hz, 4H, Ar), 6.79 (d, J = 7.8 Hz, 4H, NHCO), 5.03–4.95 (m, 4H, α-CHTrp), 3.71 (s, 12H, OCH_3), 3.36 (d, J = 5.0 Hz, 8H, β-CH_2Trp), 3.26–3.17 (m, 4H, OCH_2), 3.13–3.03 (m, 4H, OCH_2), 2.86 (d, J = 9.2 Hz, 4H, OCH_2), 2.47 (d, J = 9.2 Hz, 4H, OCH_2), 2.32–2.16 (m, 8H, CH_2). HPLC [gradient: A:B, 10-100% of A in 10 min]: 5.483 min. HRMS (ESI^+) m/z: Cald for $C_{65}H_{76}N_8O_{16}$ 1224.4857; found 1224.4836.

Tetramer 25. Following the general C2 arylation procedure, compound **24** (120 mg, 0.098 mmol), methyl 3-iodobenzoate (205.3 mg, 0.783 mmol), $Pd(OAc)_2$ (2.2 mg, 0.01 mmol,), $AgBF_4$ (152.4 mg, 0.783 mmol) and TFA (30 μL, 0.392 mmol) afforded 67.4 mg (39%) of **25** as an amorphous solid of cream color. ^{1}H NMR (300 MHz, $CDCl_3$) δ: 9.31 (bs, 4H, NH-1^{i}Trp), 8.26 (bs, 4H, Ar), 7.99–7.92 (m, 4H, Ar), 7.79–7.72 (m, 4H, Ar), 7.56–7.48 (m, 4H, Ar), 7.44 (t, J = 7.7 Hz, 3H, Ar), 7.22–7.14 (m, 4H, Ar), 7.11–6.98 (m, 8H, Ar), 6.58 (d, J = 7.9 Hz, 4H, NHCO), 4.95–4.84 (m, 4H, α-CHTrp), 3.90 (bs, 12H, OCH_3), 3.58–3.41 (m, 8H, β-CH_2Trp), 3.31 (bs, 12H, OCH_3), 3.04–2.93 (m, 4H, OCH_2), 2.92–2.82 (m, 4H, OCH_2), 2.58 (d, J = 9.3 Hz, 4H, OCH_2), 2.40 (d, J = 9.3 Hz, 4H, OCH_2), 2.05–1.95 (m, 8H, CH_2). HPLC [gradient: A:B, 10-

100% of A in 10 min]: 6.382 min. HRMS (ESI^+) m/z: Cald for $C_{97}H_{100}N_8O_{24}$ 1760.5598; found 1760.5602.

Tetramer 26. Following the general C2 arylation procedure, compound **24** (100 mg, 0.082 mmol), methyl 4-iodobenzoate (171.1 mg, 0.653 mmol), $Pd(OAc)_2$ (1.8 mg, 0.008 mmol,), $AgBF_4$ (127.1 mg, 0.653 mmol) and TFA (25 µL, 0.326 mmol) gave 46.2 mg (32%) of **26** as an amorphous solid of cream color. ^1H NMR (300 MHz, $CDCl_3$) δ: 9.39 (s, 4H, NH-1^{i}Trp), 8.07–7.98 (m, 8H, Ar), 7.68–7.58 (m, 8H, Ar), 7.56–7.47 (m, 4H, Ar), 7.16–6.99 (m, 12H, Ar), 6.55 (d, J = 7.7 Hz, 3H, NHCO), 4.93–4.84 (m, 4H, α-CHTrp), 3.90 (s, 12H, OCH_3), 3.63–3.43 (m, 8H, β-CH_2Trp), 3.36 (d, J = 3.9 Hz, 12H, OCH_3), 2.98–2.88 (m, 4H, OCH_2), 2.87–2.76 (m, 4H, OCH_2), 2.62 (d, J = 9.3 Hz, 4H, OCH_2), 2.47 (d, J = 9.2 Hz, 4H, OCH_2), 2.03–1.82 (m, 8H, CH_2). HPLC [gradient: A:B, 10-100% of A in 10 min]: 8.246 min. HRMS (ESI^+) m/z: Cald for $C_{97}H_{100}N_8O_{24}$ 1760.5598; found 1760.5600.

Tetramer 27. Following the general C2 arylation procedure, compound **24** (120 mg, 0.098 mmol), dimethyl 5-iodoisophthalate (251 mg, 0.783 mmol), $Pd(OAc)_2$ (2.2 mg, 0.010 mmol), $AgBF_4$ (152.4 mg, 0.783 mmol) and TFA (30 µL, 0.392 mmol) gave 51.7 mg (26%) of **27** as an amorphous solid of cream color. ^1H NMR (300 MHz, $CDCl_3$) δ: 9.45 (bs, 4H, NH-1^{i}Trp), 8.57 (bs, 4H, Ar), 8.43 (d, J = 1.6 Hz, 8H, Ar), 7.56–7.50 (m, 4H, Ar), 7.21–7.15 (m, 4H, Ar), 7.10–6.98 (m, 8H, Ar), 6.62 (d, J = 8.0 Hz, 4H, NHCO), 4.99–4.87 (m, 4H, α-CHTrp), 3.91 (s, 24H, OCH_3), 3.59–3.39 (m, 8H, β-CH_2Trp), 3.31 (bs, 12H, OCH_3), 3.03–2.91 (m, 4H, OCH_2), 2.90–2.82 (m, 4H, OCH_2), 2.49 (d, J = 9.3 Hz, 4H, OCH_2), 2.31 (d, J = 9.3 Hz, 4H, OCH_2), 2.12–1.96 (m, 8H, CH_2). HPLC [gradient: A:B, 10-100% of A in 10 min]: 9.368 min. HRMS (ESI^+) m/z: Cald for $C_{105}H_{108}N_8O_{31}$ 1978.0440; found 1978.0459.

Tetramer 28. Following the general procedure for methyl ester deprotection, compound **25** (34.2 mg, 0.019 mmol) gave 32 mg (quant) of **28** as an amorphous white solid. ^{1}H NMR (400 MHz, DMSO-d_6) δ: 11.32 (s, 4H, NH-1^{i}Trp), 8.24–8.17 (m, 8H, NHCO and Ar), 7.92 (t, J = 8.5 Hz, 8H, Ar), 7.67 (d, J = 8.0 Hz, 4H, Ar), 7.58 (t, J = 7.7 Hz, 4H, Ar), 7.34 (d, J = 8.0 Hz, 4H, Ar), 7.09 (t, J = 7.5 Hz, 4H, Ar), 6.99 (t, J = 7.5 Hz, 4H, Ar), 4.63–4.55 (m, 4H, α-CHTrp), 3.42–3.24 (m, 12H, OCH_2 and β-CH_2Trp), 3.15 (dd, J = 14.2, 7.1 Hz, 4H, β-CH_2Trp), 3.07 (bs, 8H, OCH_2), 2.28–2.06 (m, 8H, CH_2). ^{13}C NMR (100 MHz, DMSO-d_6) δ: 173.7, 170.5, 167.7, 136.5, 134.8, 133.6, 132.6, 131.8, 129.4, 129.3, 128.5, 122.2, 119.5, 119.3, 111.6, 108.55, 69.2, 67.4, 53.4, 45.2, 36.1, 27.9. HPLC [gradient: A:B, 10-100% of A in 10 min]: 4.846 min. HRMS (ESI^{-}) m/z: Cald for $C_{89}H_{84}N_8O_{24}$ 1648.5598; found 1648.5609. Anal. Cal. for $C_{89}H_{84}N_8O_{24}$: C, 64.80; H, 5.13. Found: C, 64.74; H, 5.01.

Tetramer 29. Following the general procedure for methyl ester deprotection, compound **26** (35.7 mg, 0.02 mmol) gave 33 mg (quant) of **29** as an amorphous white solid. ^{1}H NMR (400 MHz, DMSO-d_6) δ: 11.32 (s, 4H, NH-1^{i}Trp), 8.25 (d, J = 8.3 Hz, 4H, NHCO), 8.03 (d, J = 8.1 Hz, 8H, Ar), 7.80 (d, J = 8.1 Hz, 8H, Ar), 7.69 (d, J = 8.0 Hz, 4H, Ar), 7.35 (d, J = 8.0 Hz, 4H, Ar), 7.11 (t, J = 7.5 Hz, 4H, Ar), 7.00 (t, J = 7.5 Hz, 4H, Ar), 4.66–4.59 (m, 4H, α-CHTrp), 3.44–3.22 (m, 12H, OCH_2 and β-CH_2Trp), 3.22–3.14 (m, 4H, β-CH_2Trp), 3.03 (bs, 8H, OCH_2), 2.27–2.09 (m, 8H, CH_2). ^{13}C NMR (100 MHz, DMSO-d_6) δ: 173.7, 170.6, 167.6, 137.4, 136.65, 134.4, 130.1, 129.6, 129.3, 128.2, 122.6, 119.7, 119.4, 111.7, 109.6, 69.2, 67.3, 53.4, 45.2, 36.1, 28.1. HPLC [gradient: A:B, 10-100% of A in 10 min]: 5.235 min. HRMS (ESI^{-}) m/z: Cald for $C_{89}H_{84}N_8O_{24}$ 1648.5598; found 1648.5589. Anal. Cal. for $C_{89}H_{84}N_8O_{24}$: C, 64.80; H, 5.13. Found: C, 64.96; H, 4.98.

Tetramer 30. Following the general procedure for methyl ester deprotection, compound **27** (31 mg, 0.016 mmol) gave 28 mg (quant) of **30** as an amorphous white solid. ^{1}H NMR (500 MHz, DMSO-d_6) δ: 11.40 (s, 4H, NH-1^{i}Trp), 8.44–8.42 (m, 4H, Ar), 8.37–8.34 (m, 8H, Ar), 8.15 (d, J = 8.0 Hz, 4H, NHCO), 7.64 (d, J = 7.9 Hz, 4H, Ar), 7.33 (d, J = 8.1 Hz, 4H, Ar), 7.11–7.06 (m, 4H, Ar), 6.01–6.95 (m, 4H, Ar), 4.55–4.48 (m, 4H, α-CHTrp), 3.39–3.23 (m, 12H, OCH_2 and β-CH_2Trp), 3.15 (dd, J = 14.4, 6.9 Hz, 4H, β-CH_2Trp), 3.09–3.02 (m, 8H, OCH_2), 2.19 (m, 4H, CH_2), 2.10 (m, 4H, CH_2). ^{13}C NMR (126 MHz, DMSO-d_6) δ: 173.4, 170.4, 167.0, 136.6, 134.2, 134.0, 133.0, 132.4, 129.1, 129.0, 122.4, 119.6, 119.4, 111.7, 108.9, 69.3, 67.4, 53.2, 45.2, 36.0, 27.6. HPLC [gradient: A:B, 10-100% of A in 10 min]: 3.756 min. HRMS (ESI$^-$) m/z: Cald for $C_{93}H_{84}N_8O_{32}$ 1824.5192; found 1824.5198. Anal. Cal. for $C_{93}H_{84}N_8O_{32}$: C, 61.18; H, 4.64. Found: C, 60.96; H, 4.44.

Trimer 31. Following the general procedure for N1 benzylation, compound **4** (200 mg, 0.23 mmol), Cs_2CO_3 (335.6 mg, 1.03 mmol) and benzyl bromide (118.9 µL, 1.03 mmol) afforded 87.2 mg (33%) of **31** as an amorphous solid of cream color. ^{1}H NMR (400 MHz, $CDCl_3$) δ: 7.52–7.47 (m, 3H, Ar), 7.30–7.20 (m, 12H, Ar), 7.15–7.04 (m, 12H, Ar), 6.90 (d, J = 2.7 Hz, 3H, Ar), 6.13–6.08 (m, 3H, NHCO), 5.25 (bs, 6H, CH_2Bn), 4.90–4.83 (m, 3H, α-CHTrp), 3.61 (s, 9H, OCH_3), 3.36–3.19 (m, 6H, β-CH_2Trp), 2.14–1.90 (m, 12H, CH_2). HPLC [gradient: A:B, 10-100% of A in 10 min]: 7.566 min. HRMS (ESI$^+$) m/z: calculated for $C_{67}H_{69}N_7O_{11}$ 1147.4586; found 1147.4581.

Trimer 32. Following the general procedure for N1 benzylation, compound **4** (200 mg, 0.23 mmol), Cs_2CO_3 (335.6 mg, 1.03 mmol) and 4-fluorobenzyl bromide (127.7 µL, 1.03 mmol) afforded 116.1 mg (42%) of **32** as an amorphous solid of cream color. ^{1}H NMR (400 MHz, $CDCl_3$) δ: 7.41-7.57 (m, 3H, Ar), 7.23–7.17 (m, 3H, Ar), 7.16–7.05 (m, 6H, Ar), 7.05–6.98 (m,

6H, Ar), 6.99–6.91 (m, 6H, Ar), 6.89 (bs, 3H, Ar), 6.22–6.09 (m, 3H, NHCO), 5.21 (s, 6H, CH_2Bn), 4.91–4.80 (m, 3H, α-CHTrp), 3.62 (s, 9H, OCH_3), 3.32–3.15 (m, 6H, β-CH_2Trp), 2.16–1.90 (m, 12H, CH_2). HPLC [gradient: A:B, 10-100% of A in 10 min]: 8.517 min. HRMS (ESI^+) m/z: calculated for $C_{67}H_{66}F_3N_7O_{11}$ 1201.4586; found 1201.4582.

Trimer 33. Following the general procedure for N1 benzylation, compound **4** (200 mg, 0.23 mmol), Cs_2CO_3 (335.6 mg, 1.03 mmol) and methyl 4-(bromomethyl)benzoate (235.03 mg, 1.03 mmol) afforded 99.8 mg (33%) of **33** as an amorphous solid of cream color. ^{1}H NMR (400 MHz, $CDCl_3$) δ*:* 7.93 (d, J = 8.3 Hz, 6H, Ar), 7.52–7.47 (m, 3H, Ar), 7.16–7.04 (m, 15H, Ar), 6.93–6.91 (m, 3H, Ar), 6.25–6.21 (m, 3H, NHCO), 5.29 (bs, 6H, CH_2Bn), 4.87 (m, 3H, α-CHTrp), 3.86 (s, 9H, OCH_3), 3.62 (m, 9H, OCH_3), 3.33–3.17 (m, 6H, β-CH_2Trp), 2.13–1.90 (m, 12H, CH_2). HPLC [gradient: A:B, 10-100% of A in 10 min]: 7.619 min. HRMS (ESI^+) m/z: calculated for $C_{73}H_{75}N_7O_{17}$ 1321. 4280; found 1321. 4278.

Trimer 34. Following the general procedure for methyl ester deprotection, compound **31** (60 mg, 0.05 mmol) gave 57.1 mg (quant) of **34** as an amorphous white solid. ^{1}H NMR (400 MHz, DMSO-d_6) δ: 8.28–8.19 (m, 3H, NHCO), 7.52 (d, J = 7.8 Hz, 3H, Ar), 7.32 (d, J = 8.1 Hz, 3H, Ar), 7.26–7.14 (m, 12H, Ar), 7.12–7.07 (m, 6H, Ar), 7.03 (t, J = 7.5 Hz, 3H, Ar), 6.97 (t, J = 7.4 Hz, 3H, Ar), 5.30 (bs, 6H, CH_2Bn), 4.50–4.43 (m, 3H, α-CHTrp), 3.15 (dd, J = 14.7, 5.4 Hz, 3H, β-CH_2Trp), 2.97 (dd, J = 14.6, 8.4 Hz, 3H, β-CH_2Trp), 2.04–1.87 (m, 12H, CH_2). ^{13}C NMR (100 MHz, DMSO) δ: 173.3, 170.6, 138.3, 136.0, 128.5, 127.9, 127.5, 127.3, 126.9, 121.3, 118.8, 118.6, 110.1, 110.0, 93.2, 53.1, 49.0, 30.7, 29.3, 27.1. HPLC [gradient: A:B, 10-100% of A in 10 min]: 7.382 min. HRMS (ESI^-) m/z: calculated for $C_{64}H_{63}N_7O_{11}$ 1105.4586; found 1105.4583. Anal. Cal. for $C_{64}H_{63}N_7O_{11}$: C, 69.49; H, 5.74. Found: C, 69.66; H, 5.99.

Trimer 35. Following the general procedure for methyl ester deprotection, compound **32** (113.9 mg, 0.09 mmol) gave 109.3 mg (quant) of **35** as an amorphous white solid. ^{1}H NMR (400 MHz, DMSO-d_6) δ: 8.27–8.21 (m, 3H, NHCO), 7.52 (d, J = 7.8 Hz, 3H, Ar), 7.33 (dd, J = 8.2, 2.1 Hz, 3H, Ar), 7.25 (s, 3H, Ar), 7.18–7.12 (m, 6H, Ar), 7.10–7.01 (m, 9H, Ar), 6.97 (t, J = 7.4 Hz, 3H, Ar), 5.30 (bs, 6H, CH_2Bn), 4.49–4.41 (m, 3H, α-CHTrp), 3.14 (dd, J = 14.7, 5.6 Hz, 3H, β-CH_2Trp), 2.98 (dd, J = 14.6, 8.2 Hz, 3H, β-CH_2Trp), 2.06–1.92 (m, 12H, CH_2). ^{13}C NMR (100 MHz, DMSO) δ: 173.3, 173.3, 170.6, 170.6, 162.6, 160.2, 135.8, 134.5, 134.5, 129.0, 128.9, 127.9, 127.4, 121.3, 118.8, 118.7, 115.4, 115.1, 110.1, 93.3, 53.2, 53.1, 48.2, 30.6, 29.3, 27.1. HPLC [gradient: A:B, 10-100% of A in 10 min]: 7.771 min. HRMS (ESI$^-$) m/z: calculated for $C_{64}H_{60}F_3N_7O_{11}$ 1159.4303; found 1159.4293. Anal. Cal. for $C_{64}H_{60}F_3N_7O_{11}$: C, 66.26; H, 5.21. Found: C, 66.65; H, 4.87.

Trimer 36. Following the general procedure for methyl ester deprotection, compound **33** (79.2 mg, 0.06 mmol) gave 73.9 mg (quant) of **36** as an amorphous white solid. ^{1}H NMR (400 MHz, DMSO-d_6) δ: 8.28–8.23 (m, 3H, NHCO), 7.82 (d, J = 7.9 Hz, 6H, Ar), 7.53 (d, J = 7.7 Hz, 3H, Ar), 7.31–7.25 (m, 6H, Ar), 7.19–7.13 (m, 6H, Ar), 7.06–6.95 (m, 6H, Ar), 5.40 (bs, 6H, CH_2Bn), 4.49–4.42 (m, 3H, α-CHTrp), 3.14 (dd, J = 14.6, 5.9 Hz, 3H, β-CH_2Trp), 3.00 (dd, J = 14.5, 7.9 Hz, 3H, β-CH_2Trp), 2.06–1.92 (m, 12H, CH_2). ^{13}C NMR (100 MHz, DMSO) δ: 173.3, 170.6, 167.1, 143.4, 135.9, 129.8, 129.6, 128.0, 127.6, 126.9, 121.4, 118.9, 118.7, 110.2, 93.3, 53.2, 48.7, 30.6, 29.3, 27.2. HPLC [gradient: A:B, 10-100% of A in 10 min]: 5.380 min. HRMS (ESI$^-$) m/z: calculated for $C_{67}H_{63}N_7O_{17}$ 1237.4280; found 1237.4279. Anal. Cal. for $C_{67}H_{63}N_7O_{17}$: C, 64.99; H, 5.13. Found: C, 64.62; H, 4.90.

Tetramer 37. Following the general procedure for N1 benzylation, compound **24** (200 mg, 0.163 mmol), Cs_2CO_3 (318.9 mg, 0.98 mmol) and methyl 4-(bromomethyl)benzoate (224.3 mg,

0.98 mmol) afforded 91.9 mg (31%) of **37** as an amorphous solid of cream color. ^{1}H NMR (300 MHz, $CDCl_3$) δ: 7.96 (d, J = 8.5 Hz, 8H, Ar), 7.58 (d, J = 7.1 Hz, 4H, Ar), 7.01–7.24 (m, 20H, Ar), 6.95 (s, 4H, Ar), 6.95–6.84 (m, 4H, NHCO), 5.30 (s, 8H, CH_2Bn), 4.97 (m, 4H, α-CHTrp), 3.90 (s, 12H, OCH_3), 3.59 (s, 12H, OCH_3), 3.52–3.40 (m, 12H, OCH_2, β-CH_2Trp), 3.33–3.24 (m, 4H, β-CH_2Trp), 3.20–3.09 (m, 8H, OCH_2), 2.42–2.30 (m, 8H, CH_2). HRMS (ESI$^+$) m/z: calculated for $C_{102}H_{109}N_7O_{24}$ 1815.6215; found 1815.6207.

Tetramer 38. Following the general procedure for methyl ester deprotection, compound **37** (74.1 mg, 0.04 mmol) gave 69.5 mg (quant) of **38** as an amorphous white solid. ^{1}H NMR (300 MHz, DMSO) δ: 8.23 (d, J = 7.3 Hz, 4H, NH). 7.80 (d, J = 7.9 Hz, 8H, Ar), 7.52 (d, J = 7.7 Hz, 4H, Ar), 7.27 (d, J = 8.1 Hz, 4H, Ar), 7.23 (s, 4H, Ar), 7.13 (d, J = 7.8 Hz, 8H, Ar), 7.05-6.98 (m, 4H, Ar), 6.94 (t, J = 7.4 Hz, 4H, Ar), 5.36 (s, 8H, CH_2Bn), 4.51–4.44 (m, 4H, α-CHTrp), 3.41-3.28 (m, 8H, OCH_2), 3.14 (dd, J = 14.5, 5.6 Hz, 4H, β-CH_2Trp), 3.07 (s, 8H, OCH_2), 2.98 (dd, J = 14.7 y 8.0 Hz, 4H, β-CH_2Trp), 2.22 (m, 8H, CH_2). ^{13}C NMR (100 MHz, DMSO) δ: 174.1, 170.7, 167.8, 143.9, 136.5, 130.6, 130.2, 128.6, 128.1, 127.4, 122.0, 119.4, 111.0, 110.6, 69.6, 67.7, 54.1, 49.3, 28.1, 22.2. HPLC [gradient: A:B, 2-100% of A in 15 min]: 3.83 min. HRMS (ESI$^-$) m/z: calculated for $C_{93}H_{92}N_8O_{24}$ 1704.6225; found 1704.6267. Anal. Cal. for $C_{93}H_{92}N_8O_{24}$: C, 65.48; H, 5.44. Found: C, 65.79; H,5.83.

Dimethyl 5-[3-[2-[((benzyloxy)carbonyl)amino]-3-methoxy-3-oxopropyl]-1H-indol-2-yl]isophthalate (40). *N*-Benzyloxycarbonyl-L-tryptophan benzyl ester **39** (1.00 g, 2.84 mmol, 1 equiv), dimethyl 5-iodoisophthalate (1.36 g, 4.26 mmol, 1.50 equiv), $Pd(OAc)_2$ (32 mg, 0.14 mmol, 5% mol), $AgBF_4$ (1.10 g, 5.68 mmol, 2 equiv) and TFA (0.22 mL, 2.84 mmol, 1.00 equiv) were placed in a microwave reactor vessel in dry DMF (15 mL). The mixture was heated under microwave irradiation (250 W) at 90 ºC for 30 min. The resulting suspension was filtered

through Whatman® filter paper 42, and the solvent was removed under vacuum. The residue was dissolved in ethyl acetate (20 mL) and washed successively with saturated $NaHCO_3$ (3 x 20 mL) and brine (3 x 20 mL). The organic phase was dried over anhydrous Na_2SO_4, filtered and evaporated to dryness. The residue was purified by Biotage HPFC (High Performance Flash Chromatography) system on reverse phase using water/acetonitrile (100:0 to 0:100) to afford compound **40** (1.09 g, 71%) as an amorphous solid of cream color. ^{1}H NMR (400 MHz, $CDCl_3$) δ: 8.62 (s, 1H, NH-1^{i}Trp), 8.39 (s, 2H, Ar), 7.63 (d, *J* = 8.0 Hz, 1H, Ar), 7.37 (d, *J* = 8.1, 1H, Ar), 7.30 (m, 3H, Ar), 7.22 (d, *J* = 7.1 Hz, 3H), 7.13 (t, *J* = 7.4 Hz, 1H, Ar), 5.20 (d, *J* = 8.3 Hz, 1H, NHCO), 4.96 (d, *J* = 12.2 Hz, 1H, CH_2Ph), 4.86 (d, *J* = 12.2 Hz, 1H, CH_2Ph), 4.67 (m, 1H, *α*-CHTrp), 3.94 (s, 6H, OCH_3), 3.54 (dd, *J* = 14.8, 6.0 Hz, 1H, *β*-CH_2Trp), 3.47 (dd, *J* = 14.8, 6.0 Hz, 1H, *β*-CH_2Trp), 3.40 (s, 3H, OCH_3).^{13} C NMR (101 MHz, $CDCl_3$) δ: 172.1, 165.9, 155.5, 136.3, 136.2, 134.0, 133.9, 133.2, 131.5, 129.8, 129.1, 128.5, 128.1, 128.0, 123.3, 120.5, 119.4, 111.3, 108.5, 66.9, 54.6, 52.7, 52.3, 27.7. HPLC [gradient: H_2O:MeCN, 30-100% of A in 10 min]: 7.805 min.

Dimethyl 5-(3-(2-amino-3-methoxy-3-oxopropyl)-1H-indol-2-yl)isophthalate (41). To a solution of compound **40** (500 mg, 0.92 mmol, 1.00 equiv) in DMF (10 mL), ammonium formate (191 mg, 3.03 mmol, 3.30 equiv) and Pd/C (10% on C; 30 wt.%) were added. After 3h, the residue was filtrated through a Whatman® filter paper 42 and the solvent was removed under reduced pressure to give 358.5 mg (89% in HPLC) of **41** as an amorphous white solid. ^{1}H NMR (400 MHz, $CDCl_3$) δ: 8.64 (s, 1H, NH-1^{i}Trp), 8.50 (m, 2H, Ar), 8.45 (s, 1H, Ar), 7.67 (d, *J* = 7.9 Hz, 1H, Ar), 7.39 (d, *J* = 7.9 Hz, 1H, Ar), 7.25 (m, 1H, Ar), 7.16 (t, *J* = 7.5 Hz, 1H, Ar), 3.98 (s, 6H, OCH_3), 3.87 (m, 1H, *α*-CHTrp), 3.59 (s, 3H, OCH_3), 3.44 (dd, *J* = 14.4, 5.1 Hz, 1H, *β*-CH_2Trp), 3.17 (dd, *J* = 14.4, 5.1 Hz, 1H, *β*-CH_2Trp), 1.75 (s, 2H, NH_2). ^{13}C NMR (101 MHz,

$CDCl_3$) δ: 175.6, 166.1, 136.3, 133.9, 133.8, 133.3, 131.5, 129.7, 129.0, 123.3, 120.3, 119.6, 111.3, 110.2, 55.4, 52.7, 52.1, 30.5. HPLC [gradient: H_2O:MeCN, 5-95% of A in 10 min]: 10.270 min.

Synthesis of trimer 22 from 41. According to the general coupling procedure, tripodal polyacid **3** (100 mg, 0.36 mmol, 1.00 equiv), HATU (494 mg, 1.30 mmol, 3.60 equiv), intermediate **41** (533 mg, 1.30 mmol, 3.60 equiv) and DIPEA (440 μL, 2.70 mmol, 7.50 equiv) afforded trimer **13** (407 mg, 85%) as an amorphous white solid. Compound **13** (248 mg, 0.12 mmol, 1.00 equiv) was treated with LiOH/H_2O (232 mg, 5.52 mmol, 18.00 equiv) as it was previously described, to afford 227 mg (quant) of **22** as an amorphous white solid. Analytical and spectroscopic data of **13** and **22** are consistent with those previously found.

Synthesis of tetramer 30 from 41. According to the general coupling procedure, tetrapodal polyacid **23** (99 mg, 0.23 mmol, 1.00 equiv), HATU (426 mg, 1.12 mmol, 4.80 equiv), intermediate **41** (460 mg, 1.12 mmol, 4.80 equiv) and DIPEA (380 μL, 2.34 mmol, 10.00 equiv) afforded tetramer **27** (350 mg, 75%) as an amorphous white solid. Compound **27** (248 mg, 0.12 mmol, 1.00 equiv) was treated with LiOH/H_2O (125 mg, 2.99 mmol, 24.00 equiv) as it was previously described, to afford 227 mg (quant) of **30** as an amorphous white solid. Analytical and spectroscopic data of **27** and **30** are consistent with those previously found.

Trimer I. Following the general procedure for methyl ester deprotection, compound **4** (100 mg, 0.11 mmol) gave 95 mg (quant) of **I** as an amorphous white solid. ^{1}H NMR (500 MHz, DMSO-d_6) δ: 10.79 (bs, 3H, NH-1^{i}Trp), 8.15 (d, J = 7.9 Hz, 3H, NHCO), 7.50 (d, J = 7.8 Hz, 3H, Ar), 7.29 (d, J = 8.1 Hz, 3H, Ar), 7.10 (d, J = 7.8 Hz, 3H, Ar), 7.01 (m, 3H, Ar), 6.94 (m, 3H, Ar), 4.51–4.45 (m, 3H, α-CHTrp), 3.13 (dd, J = 14.6, 5.2 Hz, 3H, β-CH_2Trp), 2.97 (dd, J = 14.6, 8.5 Hz, 3H, β-CH_2Trp), 1.97 (m, 12H, CH_2). ^{13}C NMR (125 MHz, DMSO) δ: 174.0, 170.1,

136.5, 127.7, 124.0, 121.3, 118.7, 118.6, 111.8, 110.6, 54.0, 31.0, 29.9, 27.6. HPLC [gradient: A:B, 10-100% of A in 10 min]: 7.020 min. HRMS (ESI^+) m/z*:* calculated for $C_{43}H_{45}N_7O_{11}$ 835.3177; found 835.3165. Anal. Cal. for $C_{43}H_{45}N_7O_{11}$: C, 61.79; H, 5.43. Found: C, 61.43; H, 5.69.

Tetramer II. Following the general procedure for methyl ester deprotection, compound **24** (100 mg, 0.082 mmol) gave 95.3 mg (quant) of **II** as an amorphous white solid. ^{1}H-NMR (300 MHz, DMSO-d_6,) δ: 10.79 (d, J = 2.4 Hz, 4H, NH-1^{i}Trp), 8.13 (d, J = 7.8 Hz, 4H, NHCO), 7.52 (d, J = 7.8 Hz, 4H, Ar), 7.31 (d, J = 8.0 Hz, 4H, Ar), 7.12 (d, J = 2.3 Hz, 4H, Ar), 7.1–7.0 (m, 4H, Ar), 7.0–6.9 (m, 4H, Ar), 4.55–4.48 (m, 4H, α-CHTrp), 3.39 (t, J = 6.8 Hz, 4H, OCH_2), 3.24–2.90 (m, 12H, β-CH_2Trp and OCH_2), 2.35–2.18 (m, 4H, CH_2). ^{13}C NMR (126 MHz, CD_3OD) δ: 175.3, 174.2, 138.0, 129.0, 124.5, 122.5, 119.9, 119.3, 112.5, 110.9, 70.6, 68.0, 45.8, 40.5, 37.4, 28.6. HPLC [gradient: A:B, 10-100% of A in 10 min]: 7.700 min. HRMS (ESI^+) m/z*:* calculated for $C_{61}H_{68}N_8O_{16}$ 1169.2550; found 1170.4815. Anal. Cal. for $C_{61}H_{69}N_8O_{16}$: C, 62.66; H, 5.86. Found: C, 62.43; H, 5.69.

BIOLOGICAL ASSAYS

Antiviral activity against HIV. The MT-4 cells used for the anti-HIV assays was a kind gift from Dr. L. Montagnier (formely at the Pasteur Institute, Paris, France) and cultured in RPMI-1640 medium (Invitrogen, Merelbeke, Belgium) supplemented with 10% Fetal Calf Serum (FCS) (Hyclone, Perbio Science, Aalst, Belgium) and 1% L-glutamine (Invitrogen). The HIV-1 strain NL4-3 was obtained from the AIDS Research and Reference Reagent Program (Division of AIDS, NIAID, NIH) and cultured in MT-4 cells. The virus stock was stored at -80°C.

The compounds were evaluated for their inhibitory activity against HIV-1 (NL4.3) and HIV-2 (ROD) infection in MT-4 cell cultures as have been described in detail earlier.[63] Briefly, MT-4 cells (50 μL, 1 × 106 cells/mL) were pre-incubated for 30 min at 37 °C with the test compounds (100 μL) in a 96-well plate. Next, the cell-line adapted HIV strains (NL4.3 and ROD) were added according to the TCID50 (50% Tissue Culture Infectious Dose) of the viral stock. After 5 days, cytopathic effect (CPE) was scored microscopically and the anti-HIV-1 activity (50% effective concentration, EC50) of each compound were calculated using a colorimetric method based in the in situ reduction of 3-(4,5-dimethylthiazol-2-yl)-5-(3-carboxymethoxyphenyl)-2-(4-sulfophenyl)-2H-tetrazolium (MTS)[64] according to the manufacturer's instructions (Promega, Leiden, The Netherlands). Assays are performed by adding a small amount of a solution that contains the tetrazolium compound MTS and an electron coupling reagent (phenazine ethosulfate; PES), directly to culture wells, incubating for 1–4 hours and then recording absorbance at 490 nm (A490) with a 96-well plate reader. The quantity of formazan product as measured by the amount of 490 nm absorbance is directly proportional to the number of living cells in culture. Cytotoxicity in MT-4 cells was measured after 5 days using the MTS/PES method.[63,64] Data are the mean ± S.D. of at least 3 independent experiments.

Time-of-addition (TOA) experiment (HIV). Time-of-addition experiment was adapted from previously reported methods.[55] Briefly, MT-4 cells were infected with HIV-1(IIIB) at an m.o.i. of 0.5. Following a one hour adsorption period, cells were washed, distributed in a 96-well tray at 100,000 cells per well and incubated at 37°C. Test compounds were added at different times (0, 1, 2, 3, 4, 5 and 6h) after infection. Product added at time point 0h, was present during the start of infection and was washed away after 1 hour. After washing, fresh product was added to maintain viral suppression throughout the rest of the experiment. HIV-1 production was

determined at 31h postinfection via a p24 enzyme-linked immunosorbent assay (Perkin Elmer, Brussels, Belgium). DS5000 was used at 1 mg/mL, AZT at 3.5 μM, compounds **22** and **30** at 20 μM.

Surface plasmon resonance (SPR) analysis (HIV). It should be noted that the binding of the viral glycoprotein gp120 with the glycosaminoglycans (GAGs) of the host cell initiates HIV infection. To mimic this viral attachment, we used a Surface Plasmon Resonance (SPR) approach in which heparin, as mimic of the host cell membrane GAGs, was bound to the sensorchip.[56] In brief, heparin was biotinylated at the reducing end and captured on a streptavidin sensor chip. Gp120 (10 nM) was injected to measure the full binding capacity of the chip. Next, gp120 (10 nM) was pre-incubated with compound **22** or **30** and injected over the chip to measure the inhibitory effect of the latter compounds on gp120-heparin interaction.

The experiments were performed at 25°C on a Biacore T200 (GE Healthcare, Uppsala, Sweden) in PBS supplemented with 5% DMSO and 0.005% (v/v) Tween20 at pH 7.4. Heparin (Iduron) was minimally biotinylated at the reducing end with biotinamidohexanoic acid hydrazide (Sigma-Aldrich). Biotinylated-heparin was extensively dialyzed to remove unreacted biotin and 880 Resonance Units (RU) were captured on a Streptavidin Sensor Chip. Recombinant gp120 HIV-1(III_B) (ImmunoDiagnostics Inc., Woburn, MA) alone (10 nM) or premixed with a concentration range of compound **22** or **30** was injected for 2 minutes at a flow rate of 10 μl/min. The Sensor chip was immediately regenerated by a single treatment with 1M NaCl in 10 mM NaOH. A reference flow was used as a control for non-specific binding and several buffer blanks were used for double referencing.

Antiviral Activity against EV-A71. The EV-A71 BrCr laboratory adapted strain and clinical isolates representative of B genogroup (B2 sub-genogroup: 11316; B5 sub-genogroup:

TW/70902/08) and C genogroup (C2 sub-genogroup: H08300 461#812; C4 subgenogroup: TW/1956/05) were used at a low multiplicity of infection (MOI) in a standardized cell-based antiviral assay. Briefly, rhabdosarcoma (RD) cells were seeded in a 96 well-plate. The day after, a serial dilution of the compounds and the virus inoculum were added to the cells. The assay plates were incubated at 37 ºC, 5% CO_2 with virus inoculum and compounds until full virus–induced cell death was observed in the untreated, infected controls (3 days post-infection). Subsequently, the antiviral effect was quantified using a colorimetric readout with 3-(4,5-dimethylthiazol-2-yl)-5-(3-carboxymethoxyphenyl)-2-(4-sulfophenyl)-2H-tetrazolium/phenazine methosulfate (MTS/PMS method) and the concentration of compound at which 50% inhibition of virus-induced cell death was observed (EC_{50}), was calculated from the antiviral dose-response curves. A similar assay setup was used to determine the adverse effect of the compound on uninfected, treated cells for calculation of the CC_{50} (concentration of compound that reduces overall cell health with 50% as determined by the MTS/PMS method). Selectivity index (SI) was calculated as the ration of CC_{50} to EC_{50}.

Time-of-drug-addition experiment (EV-A71). RD cells, grown to confluence in 96-wells assay plates, were treated with compound **22** (20 μM in 2% FBS culture medium) at selected time points 1 h before or at 1, 2, 4 h post-infection with EV-A71, BrCr (MOI of 1). Virus-infected, untreated cells were used as controls. Pirodavir (20 μM), a traditional capsid binder, was included as an entry-inhibitor reference compound. At 8 h post-infection, intracellular RNA was isolated (RNeasy Mini Kit, QIAGEN) and viral RNA levels were quantified by means of RT-qPCR.

CRYO-ELECTRON MICROSCOPY STUDIES

Virus purification. EV-A71_11316 was purified as described previously.[65] Briefly, EV-A71_11316 was propagated in HeLa cells for 24 h. The media and cells were collected and processed by freezing and thawing three times. Cell debris was pelleted by centrifugation and the supernatant was precipitated with sodium chloride and polyethylene glycol (PEG) 8000. After ultracentrifugation through a 30% sucrose buffer cushion, the pellets were resuspended and applied to a 10 to 35% K-tartrate step gradient. The virus was collected and dialyzed against 10 mM Tris, 200 mM NaCl, 50 mM $MgCl_2$, pH 7.5.

Electron microscopy data collection. EM samples were prepared and data sets were recorded at the Pennsylvania State University - Huck Institutes of the Life Sciences. Prior to incubation and vitrification of the sample, the virus buffer was exchanged to phosphate-buffered saline (PBS). Compounds **22** and **30** were incubated at 20 μM with about 80 nM of the virus at 37 °C for 1 hour, which equates to about four copies of molecule per each of vertex on the virus capsid. Three microliters of each sample were pipetted onto carbon coated Quantifoil R2/1 grids (Quantifoil Micro Tools GmbH, Jena, Germany), blotted to remove excess, and plunge-frozen in liquid ethane using a Vitrobot (Thermo Fisher, USA). Grids were imaged in a Titan Krios G3 under automated control of the FEI EPU software. An atlas image was assembled from micrographs taken at 165x magnification on a FEI BM-Ceta camera, and suitable areas were selected for imaging on the FEI Falcon 3EC direct electron detector. The microscope was operated at 300 kV with a 70 μm condenser aperture and a 100 μm objective aperture. Magnification was set at 59,000x yielding a calibrated pixel size of 1.1 Å. Images were recorded in integration mode saving 59 and 19 fraction images for **22** and **30** and the total accumulated exposure was 140 and 58 $e^-/Å^2$, respectively (Supporting Information, S1Table).

Image processing. Both data sets (EV-A71_11316-**22** and EV-A71_11316-**30**) were processed in the same manner. Micrograph movie frame stacks were aligned and dose-weighted with the UCSF program MotionCorr v2.1[66] and the contrast transfer function (CTF) of each micrograph was determined with GCTF.[67] Image processing steps were performed by using RELION v3.1.[68] After initial particle picking for a subset of the data, particles were extracted with a 420-pixel by 420-pixel box and processed for reference-free 2D classification. Using the output 2D classes as references, 51,413 and 84,522 particles were picked by automatic particle picking for **22** and **30** data sets, respectively. The extracted particles were subjected to 2D- and 3D-classification, yielding 42,926 and 30,452 particles. An *ab initio* 3D model was generated with icosahedral-symmetry averaging by a stochastic gradient descent algorithm in RELION, followed by 3D refinement. 3.45 Å and 3.42 Å resolution maps for the virus-alone and the complex (FSC = 0.143) were reconstructed after post-processing. Resolutions improved to 3.03 Å and 2.89 Å after applying CTF refinement and Bayesian polishing in Relion. In addition to the new complex data, we also reprocessed the recently published EV-A71 data set, which improved the resolution to 3.08[42] (Supporting Information, S1 Table). Specifically, 75,125 particles were selected from 152,476 after 2D and 3D classifications and CTF refinement and Bayesian polishing were applied using the same method as for the two virus-drug complex datasets. Ewald sphere correction was applied to all three maps, resulting in only marginal resolution improvements (Supporting Information, S1 Table).

Atomic coordinate refinement. An atomic model of EV-A71_11316 (PDB ID: 6DIJ)[42] was used as a starting model. Building of the model into the three sharpened maps was initiated by fitting the starting model as a rigid body in Chimera.[70] The fitted structure of an asymmetric unit was refined with additional rigid_body, morphing, and simulated_annealing options in PHENIX

real-space refinement.[71] The refinement asymmetric units were duplicated for sixty icosahedral units and refined with non-crystallographic symmetry using PHENIX real-space refinement.[71] Then, the asymmetric units were refined additionally to optimize the model geometry. The map cross-correlation values with mask for all three models were between 0.81 and 0.83. Root-mean-square deviation (RMSD) deviations from ideal bonds length and angles were 0.010 ~ 0.011 Å and 0.905 ~ 0.920° for all three models. Ramachandran outliers were 0.00%. The refined model was visually inspected, modified in COOT,[72] and validated by Molprobity.[73]

Map and structure accession numbers. The cryo-EM density maps for the EV-A71 virus and the two virus-complexes are available at the Electron Microscopy Data Bank via accession codes EMD-20766 (sharpened and unsharpened EV-A71_11316 maps), EMD-20768 (sharpened and unsharpened virus-**22** complex maps) and EMD-20769 (sharpened and unsharpened virus-**30** complex maps). The atomic coordinates for the viruses built in the two maps are available at the PDB via accession codes 6UH1 (EV-A71_11316), 6UH6 (virus-**22** complex) and 6UH7 (virus-**30** complex).

COMPUTER-ASSISTED MOLECULAR MODELING

Model building of the constituent fragments of **22** and **30** and subsequent assembly into the full dendrimers were accomplished by means of the editing facilities implemented in the molecular graphics program PyMOL[74] which was also employed for trajectory visualization and 3D figure generation. *Ab initio* geometry optimization and derivation of RESP point charges for the methyl-capped pentaerythritol core and the isophthaloyl-decorated Trp residue were achieved by means of a 6-31G* basis set and the Hartree–Fock method, as implemented in the Gaussian 09

program.[75] The standard ff14SB force field parameter set[76] in AMBER 16[77] was used for both ligand and protein atoms.

A three-dimensional cubic grid consisting of 65x65x65 points with a spacing of 0.375 Å centered on the VP1 pore region displaying electron density for **30** was defined for docking purposes. Electrostatic, desolvation, and affinity maps for the atom types present in the decorated Trp fragment of **30** were calculated using AutoGrid 4.2.6; thereafter the Lamarckian genetic algorithm implemented in AutoDock4[78] was used to generate 100 docked conformations of the fragment. Intra- and intermolecular energy evaluation of each configuration allowed the selection of the 10 best scoring solutions for each fragment. Significant clustering of top-ranking solutions at two of the five intermonomer interfaces was apparent and visual inspection confirmed their feasibility in the context of the full molecule. Therefore, the best binding poses were used for model building a complex of the VP1 pentamer with a full dendrimer that had one of its four legs docked in compliance with the previous docking results.

The VP1-**30** complex was immersed in a cubic box of TIP3P water molecules and simulated essentially as described before.[42] In brief, a weak harmonic restraint of 2 kcal mol^{-1} $Å^{-2}$ on the protein Cα atoms was used to restrain the protein backbone and every 5 ns a snapshot from the simulated trajectory was cooled down from 300 to 273 K over a 1-ns period and energy-minimized to provide an ensemble of 30 low-energy structures. The PyMOL implementation of the Adaptive Poisson-Boltzmann Solver (APBS) method[79] was used to calculate and display the molecular electrostatic potential on the solvent-accessible surface of the VP1 pentamer.

ASSOCIATED CONTENT

Supporting Information

^{1}H, ^{13}C NMR and MS spectra of the synthesized compounds (PDF) together with two-dimensional spectra of trimer **21** and tetramers **29**, **38** are included. Cryo-EM data collection, refinement and validation statistics for the EV-A71_11316 and EV-A71_11316-**22** and EV-A71_11316-**30** complexes and computer-assisted molecular modeling details. Molecular formula strings of the novel synthesized compounds are also available (CSV).

AUTHOR INFORMATION

Corresponding Author

Phone: 34912587617. Fax:34915644853. E-mail:anarosa@iqm.csic.es

ORCID

A. San-Félix: 0000-0003-4271-7598

Present Addresses

[a]Medicinal Chemistry, Rega Institute for Medical Research, KU Leuven, B-3000, Leuven, Belgium.

[b]Institute of Human Virology, Zhongshan School of Medicine, Sun Yat-sen University, Guangzhou, Guangdong, 510080, China.

[c]Department of Medicine, The Pennsylvania State University College of Medicine, Hershey, Pennsylvania, 17033, USA.

[¥] These authors contributed equally to this work

ACKNOWLEDGEMENTS

This work was supported by the Spanish Plan Nacional (Subprograma Retos) [projects SAF2015-64629-C2-1-R and SAF2015-64629-C2-2-R (MINECO/FEDER)], the Spanish "Ministerio de Ciencia, Innovación y Universidades" (project PID2019-104070RB-C21) and by the Spanish Agencia Estatal Consejo Superior de Investigaciones Científicas (CSIC, Projects CSIC-PIE-201980E100 and CSIC-PIE-201980E028), "The Centers of Excellence" of the KU Leuven (EF-05/15 and PF-10/18), EU FP7 (FP7/2007-2013) Project EUVIRNA (Grant 408 Agreement 264286), EU FP7 SILVER (Contract HEALTH-F3-2010-260644), a grant from the Belgian Interuniversity Attraction Poles (IAP) Phase VII–P7/45 (BELVIR) and the EU FP7 Industry-Academia Partnerships and Pathways Project AIROPICO. The Spanish MEC/MINECO is also acknowledged for grants to B.M-G and O.M-M. and the China Scholarship Council (CSC) (Grant 201403250056) for a grant to L.S. S.H. received a grant with the Pennsylvania Department of Health using Tobacco CURE Funds. We also thank Charlotte Vanderheydt, Sandra Claes and Evelyne Van Kerckhove for helping with the processing of the antiviral data. This work has been awarded with the Janssen (XVIII call) and Esteve (XIX call) prizes within the "Prizes for Young Researchers of the Spanish Society of Medicinal Chemistry (SEQT)."

ABBREVIATIONS

Trp, tryptophan; HATU, Hexafluorophosphate Azabenzotriazole Tetramethyl Uronium; DIPEA, N,N-diisopropylethylamine; TFA, trifluoroacetic acid; DMF, dimethylformamide; HIV, Human immunodeficiency virus; AIDS, Acquired Immune Deficiency Syndrome; FCS, fetal calf serum; GAGs, glycosaminoglycans; MTS, 3-(4,5-dimethylthiazol-2-yl)-5-(3-carboxymethoxyphenyl)-2-(4-sulfophenyl)-2H-tetrazolium; SPR, Surface plasmon resonance; PES, phenazine ethosulfate;

EV71, enterovirus 71; EV-A71, enterovirus 71 genogroup A; CCR5, chemokine receptor type 5; DS-5000, dextran sulfate-5000; PRM-A, pradimicin A; cryo-EM, cryo-electron microscopy.

PDB ID Codes. Coordinates have been deposited at the Protein Data Bank (PDB) under accession numbers PDB 6UH1 (EV-A71_11316), PDB 6UH6 (EV-A71_11316 + **22**) and PDB 6UH7 (EV-A71_11316 + **30**). Authors will release the atomic coordinates and experimental data upon article publication. PDB IDs have been provided in Table S1 (Supporting Material, page S31).

REFERENCES

(1) UNAIDS data 2018. http://www.unaids.org/en/topic/data (accessed 22 August 2019).

(2) Arts, E. J.; Hazuda, D. J. HIV-1 antiretroviral drug therapy. *Cold Spring Harbor Perspect. Med.* **2012**, *2*, a007161.

(3) Broder S. The development of antiretroviral therapy and its impact on the HIV-1/AIDS pandemic. Antiviral Res. **2010**, *85*, 1–18.

(4) De Clercq, E.; Li, G. Approved antiviral drugs over the past 50 years. *Clin. Microbiol. Rev*. **2016**, *29*, 695-747.

(5) Mehellou, Y.; De Clercq, E. Twenty-six years of anti-HIV drug discovery: where do we stand and where do we go?. *J. Med. Chem.* **2010**, *53*, 521-538.

(6) Volberding, S.; Deeks, G. Antiretroviral therapy and management of HIV infection. *Lancet* **2010**, *376*, 9734, 49-62.

(7) Zhan, P; Pannecouque, C.; De Clercq, E.; Liu, X. Anti-HIV drug discovery and development: Current innovations and future trends. *J. Med. Chem.* **2016**, *59*, 2849-2878.

(8) Drug resistance database. https://hivdb.stanford.edu/dr-summary/resistance-notes/NNRTI/ (accessed December 13, 2018).

(9) Gaardbo, J.C.; Hartling, H.J.; Gerstoft, J.; Nielsen, S.D. Incomplete immune recovery in HIV infection: mechanisms, relevance for clinical care, and possible solutions. *Clin. Dev. Immunol.* **2012**, 670957, 1-17.

(10) Margolis, A.M.; Heverling, H.; Pham, P.A.; Stolbach. A. A Review of the Toxicity of HIV Medications, *J. Med. Toxicol*. **2014**, *10*, 26-39.

(11) Rojas, P.; Holguín, A. Drug resistance in the HIV-1-infected paediatric population worldwide: a systematic review. *J. Antimicrob. Chemother.* **2014**, 69, 2032-2042.

(12) WHO. World Health Organization HIV/AIDS fact sheet [Internet]. 2018 https://www.who.int/en/news-room/fact-sheets/detail/hiv-aids (accessed 19 July 2018).

(13) Barré-Sinoussi, F.; Ross, A. L.; Delfraissy, J.-F. Past, present and future: 30 years of HIV research. *Nat. Rev. Microbiol*. **2013**, *12*, 877-883.

(14) Badia, R., Ballana, E., Esté, J.A., Riveira-Muñoz, E. Antiviral treatment strategies based on gene silencing and genome editing, *Curr. Opin. Virol,* **2017**, *24*, 46–54.

(15) Kumari, G.; Singh. R.K. Anti-HIV drug development: structural features and limitations of present day drugs and future challenges in the successful HIV/AIDS treatment. *Curr. Pharm. Des.* **2013**, *19*, 1767-1783.

(16) Tintori, C.; Brai, A.; Fallacara, A. L.; Fazi, R.; Schenone, S.; Botta. M. Protein–protein interactions and human cellular cofactors as new targets for HIV therapy. *Curr. Opin. Pharmacol.* **2014**, *18*, 1-8.

(17) Gulick, R.M., Investigational antiretroviral drugs: what is coming down the pipeline. *Top. Antivir. Med.* **2019**, *25*, 127-132.

(18) Esté, J.A. Inhibition of HIV entry. In: *Antiviral drug strategies, Methods and principles in Medicinal Chemistry*, vol 50; De Clercq, E. (Ed.); Wiley-VCH Verlag GmbH&Co. KGaA; Weinheim, Germany, 2011; pp 29-50.

(19) Kang, Y.; Guo, J.; Chen, Z. Closing the door to human immunodeficiency virus. Protein Cell **2013**, *4*, 86-102.

(20) Klase, J. The molecular basis of HIV entry. *Cell Microbiol*. **2012**, *14*, 1183–1192.

(21) Lu, L.; Fei, Y.; Lifeng, C.; Asim, K. D.; Shibo, J. Development of small-molecule HIV entry inhibitors specifically targeting gp120 or gp41. *Curr. To. Med. Chem.* **2016**, *16*, 1074–1090.

(22) Micewicz, E.D.; Ruchala, P. Inhibitors of HIV-1 entry. *Curr. Pharm. Des.,* **2013**, *10*, 1784-1799.

(23) Wilen, C.B.; Tilton, J.C.; Doms, R.W. Molecular mechanisms of HIV entry. *Adv. Exp. Med. Biol.* **2012**, *726*, 223-242.

(24) Ding, X.; Zhu, Y.; Chong, H.; Cui, S.; Zhang, X.; He, J.; Wang, X.; He, Y. Structural and functional characterization of HIV-1 cell fusion inhibitor T20. *AIDS*, **2018**, *33*, 1-11.

(25) Fletcher. C.V. Enfuvirtide, a new drug for HIV infection. *Lancet* **2003**, *361,* 1577-1578.

(26) Woollard, S.M.; Kanmogne, G.D., Maraviroc: a review of its use in HIV infection and beyond. *Drug. Des. Devel. Ther.,* **2015**, *9*, 5447-5468.

(27) Markham, A. Ibalizumab: First global approval. *Drugs*, **2018**, *78*, 781-785.

(28) Rivero-Buceta, E.; Doyagüez, E.G.; Colomer, I.; Quesada, E.; Mathys, L.; Noppen, S.; Liekens, S.; Camarasa, M-J.; Pérez-Pérez, M-J.; Balzarini. J.; San-Félix, A. Tryptophan

dendrimers that inhibit HIV replication, prevent virus entry and bind to the HIV envelope glycoproteins gp120 and gp41. *European J. Med Chem* **2015**, *106*, 34-43.

(29) Rivero-Buceta, E.; Sun, L.; Martínez-Gualda, B.; Doyagüez, E.G.; Donkers, K.; Quesada, E.; Camarasa, M-J.; Delang, L.; San-Félix, A.; Neyts, J.; Leyssen. P. Optimization of a class of tryptophan dendrimers that inhibit HIV replication leads to a selective, specific and low-nanomolar inhibitor of clinical isolates of enterovirus A71. *Antimicrob. Agents and Chemother* **2016**, *60*, 5064-5067.

(30) Nadel, S. Hand, foot, mouth, brainstem and heart disease resulting from enterovirus 71. *Crit. Care Med.,* **2013,** *41*, 1821-1822.

(31) Solomon, T.; Lewthwaite, P.; Perera, D.; Cardosa, M.J.; McMinn, P.; Ooi, M.H. Virology, epidemiology, pathogenesis and control of enterovirus 71. *Lancet Infect.Dis.*, **2010**, *10*, 778-790.

(32) McMinn, P.C. An overview of the evolution of enterovirus 71 and its clinical and public health significance. *FEMS Microbiol Rev.* **2002**, *26*, 91-107.

(33) Chang, L-Y.; Huang, L-M.; Gau, SS-F.; Wu, Y-Y.; Hsia, S-H.; Fan, T-Y.; Lin, K-L.; Huang, Y-C.; Lu, C-Y.; Lin, T-Y. Neurodevelopment and cognition in children after enterovirus 71 infection. *N. Engl. J. Med.* **2007**, *356*, 1226–1234.

(34) Chen, C.Y.; Chang, Y.C.; Huang, C.C.; Lui, C.C.; Lee, K.W.; Huang. S.C. Acute flaccid paralysis in infants and young children with enterovirus 71 infection: MR imaging findings and clinical correlates. *AJNR Am. J. Neuroradiol.* **2001**, *22*, 200–205.

(35) Chan, Y-F.; Sam, I-C.; Wee, K-L.; Abubakar, S. Enterovirus 71 in Malaysia: A decade later. *Neurol Asia*, **2011**, *16*, 1-15.

(36) ProMED-mail post Human enterovirus 2016 Spain: (CT) http://promedmail.org/post/20160524.4242904 for earlier report on this enterovirus outbreak in Catalonia, Spain.

(37) ECDC [European Centre for Disease Prevention and Control] Week 31, 29 July-4 August 2018 https://ecdc.europa.eu/en/search?s=enterovirus+A71

(38) Tan, Y.W.; Chu, J.J.H. Sinovac EV71 vaccine: the silver bullet for hand,foot and mouth disease-or not? *J. Public Heal Emerg.* **2017**; 1. doi: 10.21037/jphe.2016.12.14.

(39) Li, J.X.; Song, Y.F.; Wang, L.; Zhang,, XF, Hu YS, Hu, YM, Xia, JL, Li, J, Zhu, FC, Two-year efficacy and immunogenicity of Sinovac Enterovirus 71 vaccine agasint hand, foot and mouth disease in children, *Expert Rev, Vaccines* **2016**, *15*, 129-137.

(40) Ng, Q.; He, F.; Kwang, J. Recent progress towards novel EV71 anti-therapeutics and vaccines. *Viruses* **2015**, *7*, 6441–6457.

(41) Baggen, J.; Thibaut, H.J.; Strating J.R.P.M., van Kuppeveld, F.J.M.. The life cycle of non-polio enteroviruses and how to target it. *Nat. Rev. Microbiol.* **2018**, *16,* 368-381.

(42) Sun, L.; Lee, H.; Thibaut, H.J; Rivero-Buceta, E.; Bator, C.; Martinez-Gualda, B. ; Dallmeiera, K.; Leen Delang, L.; Leyssen, P.; Gago, F.; San-Félix A.; Hafenstein, S.; Mirabelli, C.; Neyts J., 2019. Viral engagement with host (co-)receptors blocked by a novel class of tryptophan dendrimers that targets the 5-fold-axis of the enterovirus-A71 capsid. PLOS Pathog. 15(5), e1007760.htps//doi.org/10.1371/journal.ppat/1007760.

(43) Martínez-Gualda,B.; Sun, L.; Rivero-Buceta, E.; Flores, A.; Quesada, E.; Balzarini, J.; Noppen, S.; Liekens, S.; Schols, D.; Neyts, J.; Leyssen, P.; Mirabelli, C.; Camarasa, M.J.; San-Félix, A. Structure-activity relationship studies on a Trp dendrimer with dual activities

against HIV and enterovirus A71. Modifications on the amino acid. *Antivir. Res*. **2017,** *139*, 32-40.

(44) Martínez-Gualda,B.; Sun, L.; Martí-Marí, O.; Mirabelli, C.; Delang, L.; Neyts, J.; Schols, D.; Camarasa, M.-J., San-Félix, A. Modifications in the branched arms of a class of dual inhibitors of HIV and EV71 replication expand their antiviral spectrum. *Antivir. Res.* **2019**, 210-214.

(45) Cachi, S.; Fabrizi, G. Synthesis and functionalization of indoles through palladium-catalyzed reactions. *Chem. Rev.* **2005**, 2873-2920.

(46) Ruiz-Rodríguez, J.; Albericio, F.; Lavilla, R. Post-synthetic modification of peptides: chemoselective C-arylation of tryptophan residues. *Chem. Eur. J.* **2010**, *16*, 1124-1127.

(47) Preciado, S.; Mendive-Tapia, L.; Albericio, F.; Lavilla, R. Synthesis of C-2 arylated tryptophan amino acids and related compounds through palladium-catalyzed C-H activation. *J. Org. Chem.,* **2013,** *78,* 8129-8135.

(48) Ornelas, C.; Broichhagen, J.; Weck, M. Strain-promoted alkyne azide cycloaddition for the functionalization of poly(amide)-based dendrons and dendrimers. *J. Am. Chem. Soc*., **2010**, *132*, 3923-3931.

(49) Flores, A.; Camarasa, M.J.; Pérez-Pérez, M.J.; San-Félix, A.; Balzarini, J.; Quesada, E. Multivalent agents containing 1-substituted 2,3,4-trihydroxyphenyl moieties as novel synthetic polyphenols directed against HIV-1. *Org. Biomol. Chem.* **2014**, *12*, 5278-5294.

(50) Newkome, G.R.; Weis, C.D. 6,6-bis(carboxy-2-oxabutyl)-4,8-dioxaundecane-1,11-dicarboxylic acid. *Org. Prep. Proced. Int.,* **1996**, *28*, 242-244.

(51) Gowda, D.Ch.; Rajesh, B.; Gowda, S. Ammonium formate catalytic transfer hydrogenation: a convenient method for removal of halogenated benzyloxycarbonyl and benzyl protecting groupd in peptide synthesis, *Indian Journal of Chemistry*, **2000**, 39B, 504-508.

(52) Baba, M.; Pauwels, R.; Balzarini, J.; Arnout, J.; Desmyter, J.; De Clercq, E. Mechanism of inhibitory effect of dextran sulfate and heparin on replication of human immunodeficiency virus in vitro. *Proc. Natl. Acad. Sci.* **1988**, *85*, 6132-6136.

(53) Balzarini, J.; Laethem, K.V.; Daelemans, D.; Hatse, S.; Bugatti, A.; Rusnati, M.; Igarashi, Y.; Oki, T.; Schols, D. Pradimicin A, a carbohydrate-binding nonpeptidic lead compound for treatment of infections with viruses with highly glycosylated envelopes, such as human Immunodeficiency virus, *J. Virol*. **2007**, *81*, 362-373.

(54) Pauwels, R.; Andries, K.; Desmyter, J.; Schols, D.; Kukla, M. J.; Breslin, H. J.; Raeymaeckers, A.; Van Gelder, J.; Woestenborghs, R.; Heykants, J.; Schellekens, K.; Janssen, M. A. C.; De Clercq, E. and Janssen, P.A.J. Potent and selective inhibition of HIV-1 replication in vitro by a novel series of TIBO derivatives. *Nature* **1990**, 343, 470-474.

(55) Daelemans, D.; Pauwels, R.; De Clercq, E. and Pannecouque, C. A time-of-drug addition approach to target identification of antiviral compounds. *Nat. Protoc.* **2011**, *6*, 925-933.

(56) Nici, F; Oliviero, G.; Falanga, A.P.; D'Errico, S.; Marzano, M.; Musumeci, D.; Montesarchio, D.; Noppen, S.; Pannecouque, C.; Piccialli, G.; Borbone, N. Anti-HIV activity of new higher order G-quadruplex aptamers obtained from tetra-end-linked oligonucleotides. *Org. Biomol. Chem.* **2018**, *16*, 2349-2355.

(57) Tijsma, A.; Franco, D.; Tucker, S.; Hilgenfeld, R.; Froeyen, M.; Leyssen, P.; Neyts, J. The capsid binder vapendavir and the novel protease inhibitor SG85 inhibit enterovirus 71 replication. *Antimicrob. Agents Chemother.* **2014**, *58*, 6990–6992.

(58) Andries, K.; Dewindt, B.; Snoeks, J.; Willebrords, R.; Van Eemeren, K.; Stokbroekx, R.; Janssen, P.A.J. In vitro activity of pirodavir (R 77975), a substituted phenoxy pyridazinamine with broad-spectrum antipicornaviral activity. *Antimicrob Agents Chemother,* **1992**, *36*, 100–107.

(59) Yamayoshi, S.; Yamashita, Y.; Li, J.; Hanagata, N.; Minowa, T.; Takemura, T.; Koike, S. Scavenger receptor B2 is a celular receptor for enterovirus **2009**, *Nat. Med*. *15*, 798-801.

(60) Thibaut, H.J.; Leyssen, P.; Puerstinger, G.; Muigg, A.; Neyts, J.; De Palma, A.M. Towards the design of combination therapy for the treatment of enterovirus infections. *Antiviral Res*. **2011,** *90*, 213-217.

(61) Plevka, P; Perera, R.; Cardosa, J.; Kuhn, R.J.; Rossman, M.G. Crystal structure of human enterovirus 71, *Science.* **2012** *336,* 1274.

(62) Plevka, P; Perera, R.; Cardosa, J.; Kuhn, R.J.; Rossman, M.G. Structure determination of enterovirus 71. *Acta Cryst.* **2012**, 1217-1222.

(63) Vermeire, K.; Princen, K.; Hatse, S.; De Clercq, E.; Dey. K; Bell; T.W.; Schols, D. CADA, a novel CD4-targeted HIV inhibitor, is synergistic with various anti-HIV drugs in vitro. AIDS **2004**, *18*, 2115–2125.

(64) Pauwels, R.; Balzarini, J.; Baba, M.; Snoeck, R.; Schols, D.; Herdewijn, P.;Desmyter, J.; De Clercq, E. Rapid and automated tetrazolium-based colorimetric assay for the detection of anti-HIV compounds. *J. Virol. Meth.,* **1988**, *20*, 309–321.

(65) Shingler, K. L.; Organtini, L. J.; Hafenstein, S. Enterovirus 71 Virus Propagation and Purification. *Bio-protocol* **2014**, *4*, 9, DOI: 10.21769/BioProtoc.1117.

(66) Zheng, S. Q.; Palovcak, E.; Armache, J.P.; Verba, K.A.; Cheng, Y.; Agard, D.A. MotionCor2: anisotropic correction of beam-induced motion for improved cryo-electron microscopy. *Nat. Methods* **2017**, *14,* 331–332.

(67) Zhang, K. Gctf: Real-time CTF determination and correction. *J. Struct. Biol.* **2016**, *193*, 1–12.

(68) Zivanov, J.; Nakane T.; Forsberg B.O.; Kimanius D.; Hagen W.J.H.; Lindahl E.; Scheres S.H.W. New tools for automated high-resolution cryo-EM structure determination in RELION-3. *eLife* **2018,** 7:e42166 DOI: 10.7554/eLife.42166.

(69) Scheres, S. H. W. Semi-automated selection of cryo-EM particles in RELION-1.3. *J. Struct. Biol.* **2015**, *189*, 114–122.

(70) Pettersen, E. F.; Goddard, T.D.; Huang, C.C.; Couch, G.S.; Greenblatt, D.M.; Meng, E.C.; Ferrin, T.E. UCSF Chimera—A visualization system for exploratory research and analysis. *J. Comput.Chem.* **2004**, *25*, 1605–1612.

(71) Afonine, P.V.; Headd, J.J.; Terwilliger, T. C.; Adams, P. D. PHENIX News. *Computational Crystallography Newsletter* **2013**, *4*, 43–44.

(72) Emsley, P.; Lohkamp, B.; Scott, W. G.; Cowtan, K. Features and development of Coot. *Acta Crystallogr. D Biol. Crystallogr.* **2010,** *66,* 486–501.

(73) Chen, V.B.; Arendall W.B.3rd; Headd J.J.; Keedy, D.A. Immormino, R.M.; Kaprai G.J.; Murray, L.W.; Richarson, J.S.; Richardson D.C. *MolProbity*: all-atom structure validation for macromolecular crystallography. *Acta Crystallogr. D Biol. Crystallogr.* 2010, **66**, 12–21.

(74) DeLano, W. L. *The PyMOL Molecular Graphics System*, 1.3; Schrödinger, LLC.: **2013**.

(75) Frisch MJ, Trucks GW, Schlegel HB, Scuseria GE, Robb MA, Cheeseman JR, Scalmani G, Barone V, Mennucci B, Petersson GA, Nakatsuji H, Caricato M, Li X, Hratchian HP, Izmaylov AF, Bloino J, Zheng G, Sonnenberg JL, Hada M, Ehara M, Toyota K, Fukuda R, Hasegawa J, Ishida M, Nakajima T, Honda Y, Kitao O, Nakai H, Vreven T, Montgomery JA Jr, Peralta JE, Ogliaro F, Bearpark MJ, Heyd J, Brothers EN, Kudin KN, Staroverov VN, Kobayashi R, Normand J, Raghavachari K, Rendell AP, Burant JC, Iyengar SS, Tomasi J, Cossi M, Rega N, Millam NJ, Klene M, Knox JE, Cross JB, Bakken V, Adamo C, Jaramillo J, Gomperts R, Stratmann RE, Yazyev O, Austin AJ, Cammi R, Pomelli C, Ochterski JW, Martin RL, Morokuma K, Zakrzewski VG, Voth GA, Salvador P, Dannenberg JJ, Dapprich S, Daniels AD, Farkas Ö, Foresman JB, Ortiz JV, Cioslowski J, Fox DJ **(2009**) Gaussian 09, Gaussian, Inc., Wallingford

(76) Maier, J. A.; Martinez, C.; Kasavajhala, K.; Wickstrom, L.; Hauser, K. E.; Simmerling, C., ff14SB: Improving the accuracy of protein side chain and backbone parameters from ff99SB. *J Chem Theory Comput* **2015,** *11* (8), 3696-3713.

(77) Kaus, J. W.; Pierce, L. T.; Walker, R. C.; McCammon, J. A., Improving the efficiency of free energy calculations in the AMBER molecular dynamics package. *J Chem Theory Comput* **2013,** *9* (9), 4131-4139.

(78) Morris, G. M.; Huey, R.; Lindstrom, W.; Sanner, M. F.; Belew, R. K.; Goodsell, D. S.; Olson, A. J., AutoDock4 and AutoDockTools4: Automated docking with selective receptor flexibility. *J. Comput. Chem.* **2009,** *30*, 2785-2791.

(79) Baker, N. A.; Sept, D.; Joseph, S.; Holst, M. J.; McCammon, J. A., Electrostatics of nanosystems: application to microtubules and the ribosome. *Proc Natl Acad Sci U S A* **2001,** *98*, 10037-10041.

LIST OF CAPTIONS

Figure 1. Structures of the prototype pentaerythritol derivative **MADAL-385** (**1)** and "truncated" analogues **I** and **II**.

Figure 2. Results of the time-of-drug-addition experiment for compounds **22** and **30.** $CD4^+$ T cells were treated with the compounds at selected times before, during or after infection with HIV-1. 8h post-infection, cells were harvested and p24 was isolated and quantified by means of RT-qPCR. Data for AZT are given as reference.

Figure 3. Inhibition of gp120-heparin binding by **22** and **30** as measured by SPR. Biotinylated heparin was captured on a Streptavidin Sensor Chip. Gp120 (10 nM) was mixed with a concentration range of compound **22** (A) or **30** (B). One representative sensorgram per compound out of three independent experiments is shown. Binding levels (RU) were converted into percentage inhibition relative to gp120 binding without compound. Mean (+SEM) and nonlinear fit of three independent experiments are shown (C).

Figure 4. Time-of-drug-addition for compound **22.** RD cells were treated with the compounds at selected times before, during or after infection with EV-A71. 8h post-infection, cells were harvested and intracellular viral RNA was isolated and quantified by means of RT-qPCR.

Figure 5. Cryo-EM 3D maps identified the MADAL drugs on the capsid 5-fold vertex. (A) Surface rendering of the sharpened 3D maps for EV-A71 incubated with **22** (left) and **30** (right) showed canonical features of the capsid. Icosahedral symmetry axes were marked with arrows. **(B)** Comparison of the unsharpened maps (gray) of **22** and **30** complexes with EV-A71 showed extra densities (yellow) on the 5-fold axis. The surface rendered at 1σ and 1.9σ (insets) for EV-A71 (left), **22** (middle) and **30** (right). **(C)** Central sections of the three cryo-EM maps showed extra densities on the 5-fold-vertex covering the hole at the symmetry axis. Icosahedral symmetry axes were marked.

Figure 6. Atomic model built into the cryo-EM map. (A) The atomic models for EV-A71 VP1 (blue), VP2 (green), VP3 (red), VP4 (yellow), and the pocket factor (orange) were built into the cryo-EM map of the virus-**30** complex (gray mesh). **(B)** Representative residues of each VP and the pocket-factor are shown within the corresponding cryo-EM density envelopes to illustrate the quality of the 3D map.

Figure 7. The drug densities are connected to two VP1 residues. (A) The icosahedrally averaged drug density (yellow, **30)** was connected mostly with Lys244 and Tyr245 on the VP1 surface (grey). The atomic model of VP1 is depicted as a blue ribbon and the side-chains are shown as sticks. The surface is rendered at 1.9σ. Neighboring residues are also labeled. **(B)** Side-view of the interaction site shows the thin drug density connected to the two VP1 residues. **(C)** Binding pose proposed by the automated docking program for the substituted Trp residue in **30** at the interface between chains E (cyan) and Q (pink) using the coordinates deposited in PDB entry 6UH7.

Figure 8. Proposed binding mode of the decorated Trp moiety of 30 around the 5-fold axis of the EV-A71 capsid, as deposited in PDB entry 6UH7. (A) A semitransparent surface envelops the five VP1 chains making up the pore. C atoms in chains A, E, I, M, and Q are colored in green, cyan, magenta, yellow and pink, respectively. Note that the ethylene linker points towards the central pore. **(B)** Solvent-accessible surface of the VP1 pentamer color-coded according to the molecular electrostatic potential calculated with APBS (red, -3.0 kT/e; blue, +3.0 kT/e). The yellow surface filling the subunit interfaces corresponds to the van der Waals surface of the five docked fragments shown in (**A**).

Scheme 1. Synthesis of the tripodal derivatives **I** and **14-22**.

Scheme 2. Synthesis of the tetrapodal derivatives **II** and **28-30**.

Scheme 3. Synthesis of the N1 substituted tripodal (**34–36)** and tetrapodal (**38)** derivatives.

Scheme 4. Alternative synthetic route for the synthesis of **22** and **30**.

Table 1. Anti-HIV-1 and anti-HIV-2 activity of the selected group of compounds

Table 2. Antiviral activity of dendrimers against the BrCr lab strain of EV-A71 virus in RD cells.

Table 3. Evaluation of the broad-spectrum antiviral effect of compounds **22**, **28** and **30** against a representative panel of clinical EV71 isolates in RD cells.

Table 4. Susceptibility of reverse-engineered EV-A71 variants to prototype **1** and compounds **22** and **30**

TABLE OF CONTENTS GRAPHIC

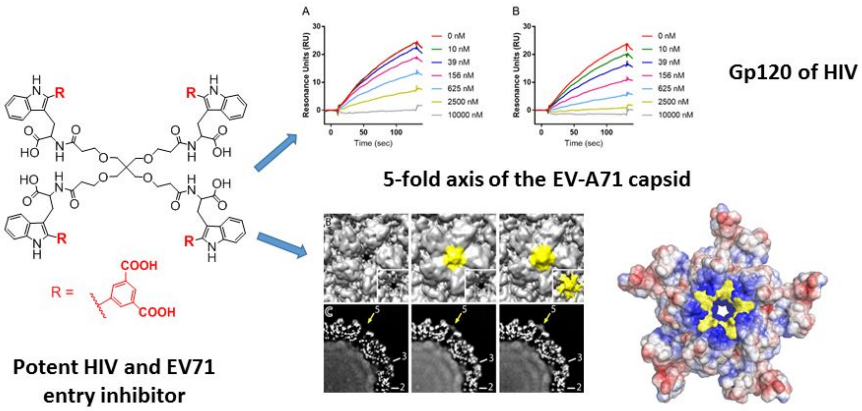

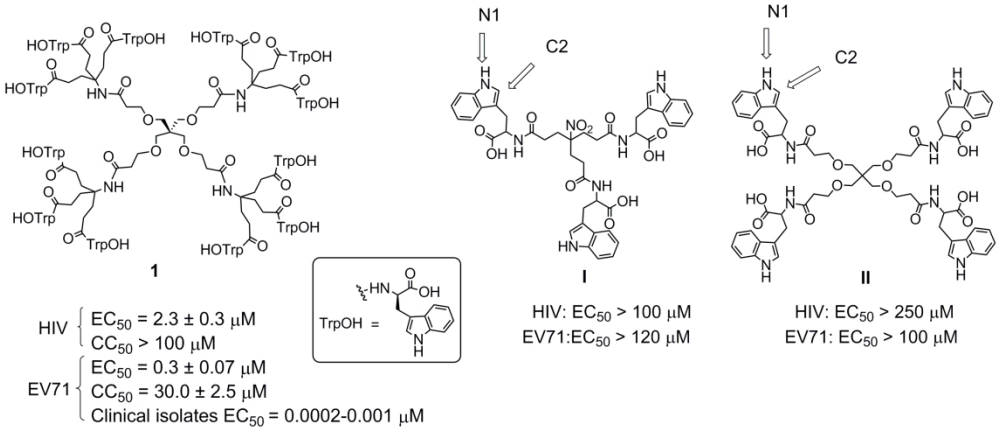

Figure 1. Structures of the prototype pentaerythritol derivative MADAL-385 (1) and "truncated" analogues I and II.

219x94mm (300 x 300 DPI)

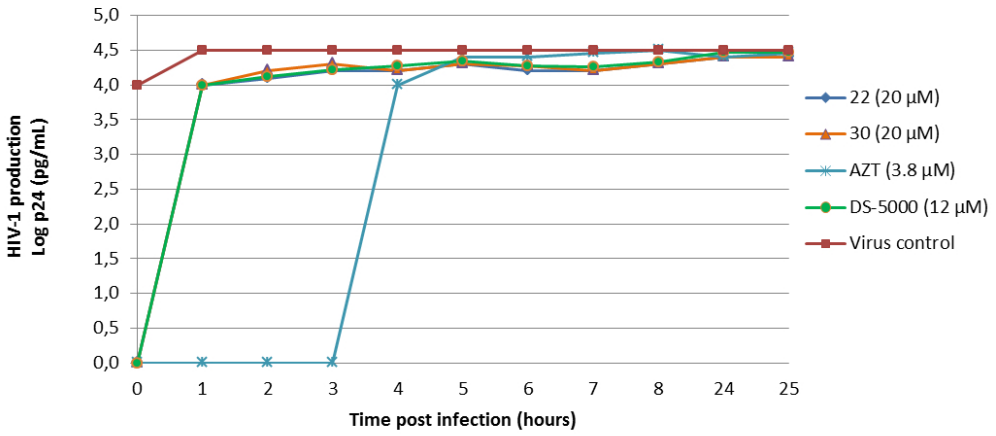

Figure 2. Results of the time-of-drug-addition experiment for compounds 22 and 30. CD4+ T cells were treated with the compounds at selected times before, during or after infection with HIV-1. 8h post-infection, cells were harvested and p24 was isolated and quantified by means of RT-qPCR. Data for AZT are given as reference.

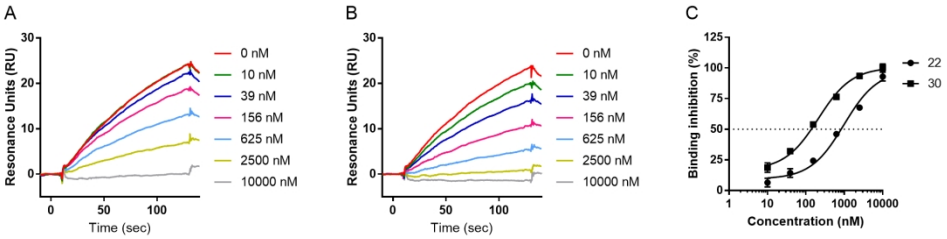

Figure 3. Inhibition of gp120-heparin binding by 22 and 30 as measured by SPR. Biotinylated heparin was captured on a Streptavidin Sensor Chip. Gp120 (10 nM) was mixed with a concentration range of compound 22 (A) or 30 (B). One representative sensorgram per compound out of three independent experiments is shown. Binding levels (RU) were converted into percentage inhibition relative to gp120 binding without compound. Mean (+SEM) and nonlinear fit of three independent experiments are shown (C).

188x53mm (300 x 300 DPI)

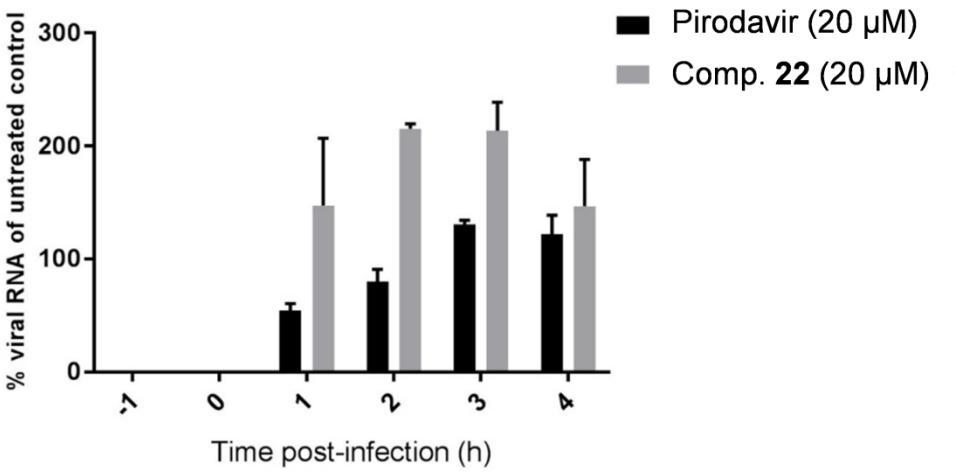

Figure 4. Time-of-drug-addition for compound 22. RD cells were treated with the compounds at selected times before, during or after infection with EV-A71. 8h post-infection, cells were harvested and intracellular viral RNA was isolated and quantified by means of RT-qPCR.

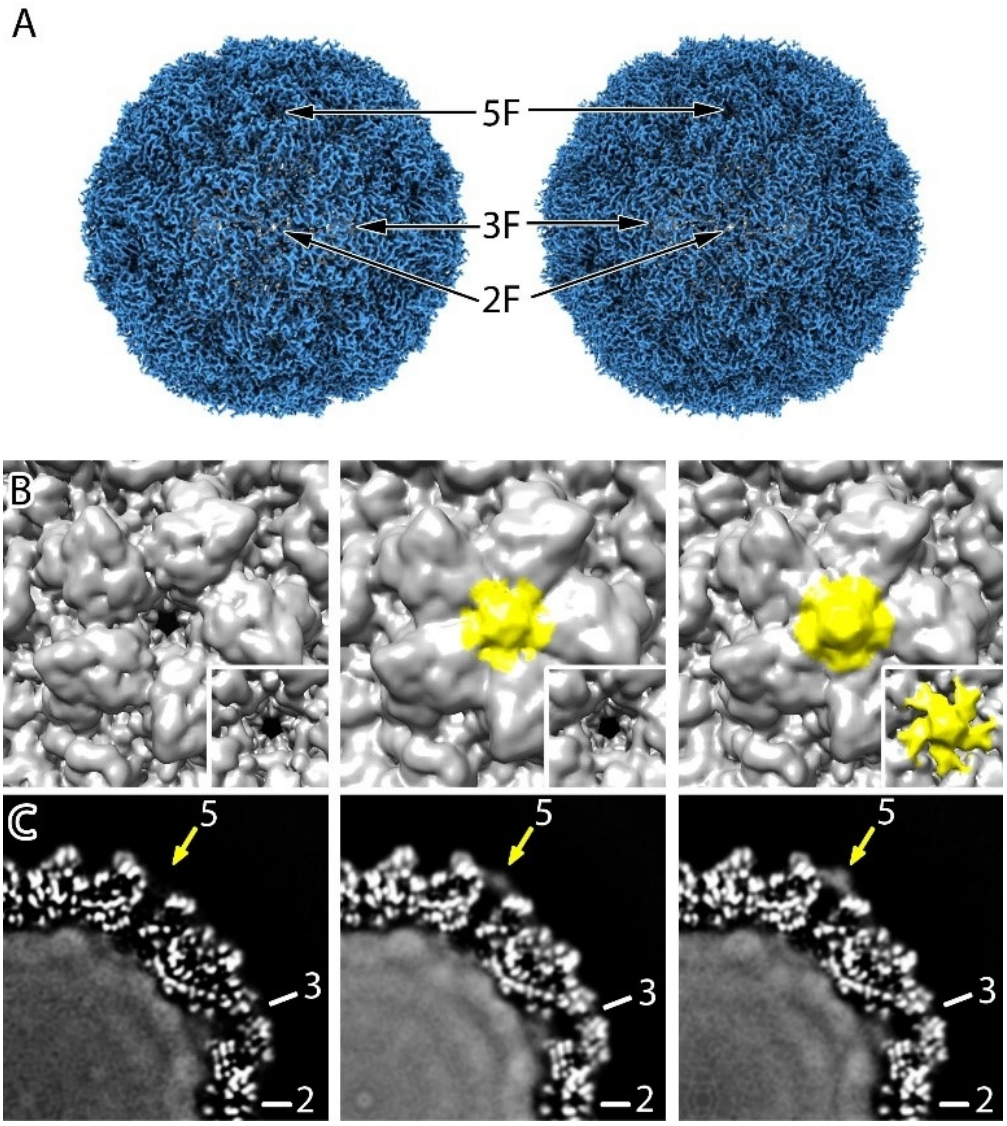

Figure 5. Cryo-EM 3D maps identified the MADAL drugs on the capsid 5-fold vertex. (A) Surface rendering of the sharpened 3D maps for EV-A71 incubated with 22 (left) and 30 (right) showed canonical features of the capsid. Icosahedral symmetry axes were marked with arrows. (B) Comparison of the unsharpened maps (gray) of 22 and 30 complexes with EV-A71 showed extra densities (yellow) on the 5-fold axis. The surface rendered at 1□ and 1.9□ (insets) for EV-A71 (left), 22 (middle) and 30 (right). (C) Central sections of the three cryo-EM maps showed extra densities on the 5-fold-vertex covering the hole at the symmetry axis. Icosahedral symmetry axes were marked.

89x99mm (220 x 220 DPI)

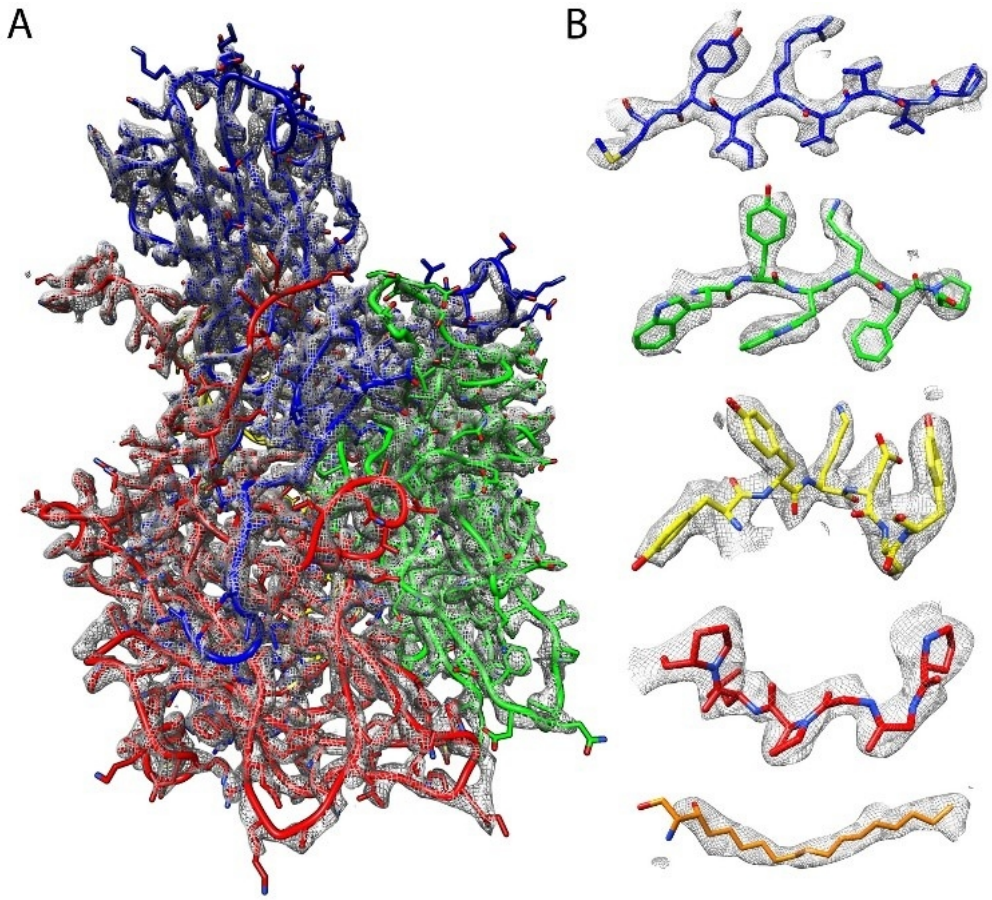

Figure 6. Atomic model built into the cryo-EM map. (A) The atomic models for EV-A71 VP1 (blue), VP2 (green), VP3 (red), VP4 (yellow), and the pocket factor (orange) were built into the cryo-EM map of the virus-30 complex (gray mesh). (B) Representative residues of each VP and the pocket-factor are shown within the corresponding cryo-EM density envelopes to illustrate the quality of the 3D map.

86x78mm (220 x 220 DPI)

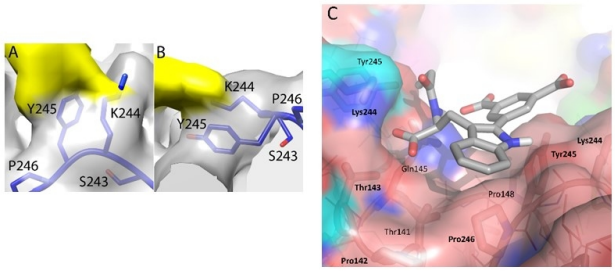

Figure 7. The drug densities are connected to two VP1 residues. (A) The icosahedrally averaged drug density (yellow, 30) was connected mostly with Lys244 and Tyr245 on the VP1 surface (grey). The atomic model of VP1 is depicted as a blue ribbon and the side-chains are shown as sticks. The surface is rendered at 1.9□. Neighboring residues are also labeled. (B) Side-view of the interaction site shows the thin drug density connected to the two VP1 residues. (C) Binding pose proposed by the automated docking program for the substituted Trp residue in 30 at the interface between chains E (cyan) and Q (pink) using the coordinates deposited in PDB entry 6UH7.

338x190mm (96 x 96 DPI)

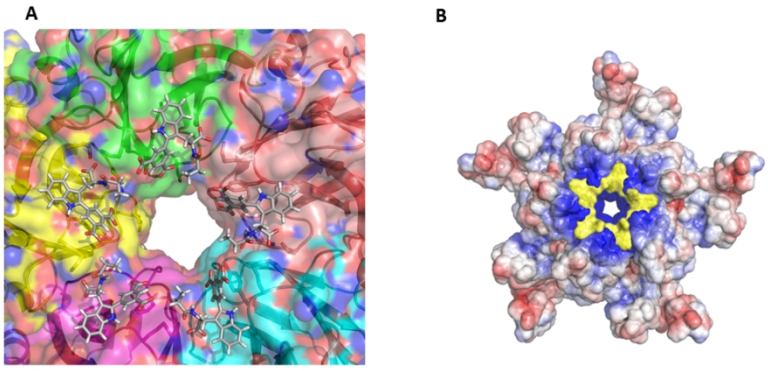

Figure 8. Proposed binding mode of the decorated Trp moiety of 30 around the 5-fold axis of the EV-A71 capsid, as deposited in PDB entry 6UH7. (A) A semitransparent surface envelops the five VP1 chains making up the pore. C atoms in chains A, E, I, M, and Q are colored in green, cyan, magenta, yellow and pink, respectively. Note that the ethylene linker points towards the central pore. (B) Solvent-accessible surface of the VP1 pentamer color-coded according to the molecular electrostatic potential calculated with APBS (red, -3.0 kT/e; blue, +3.0 kT/e). The yellow surface filling the subunit interfaces corresponds to the van der Waals surface of the five docked fragments shown in (A).

338x190mm (96 x 96 DPI)

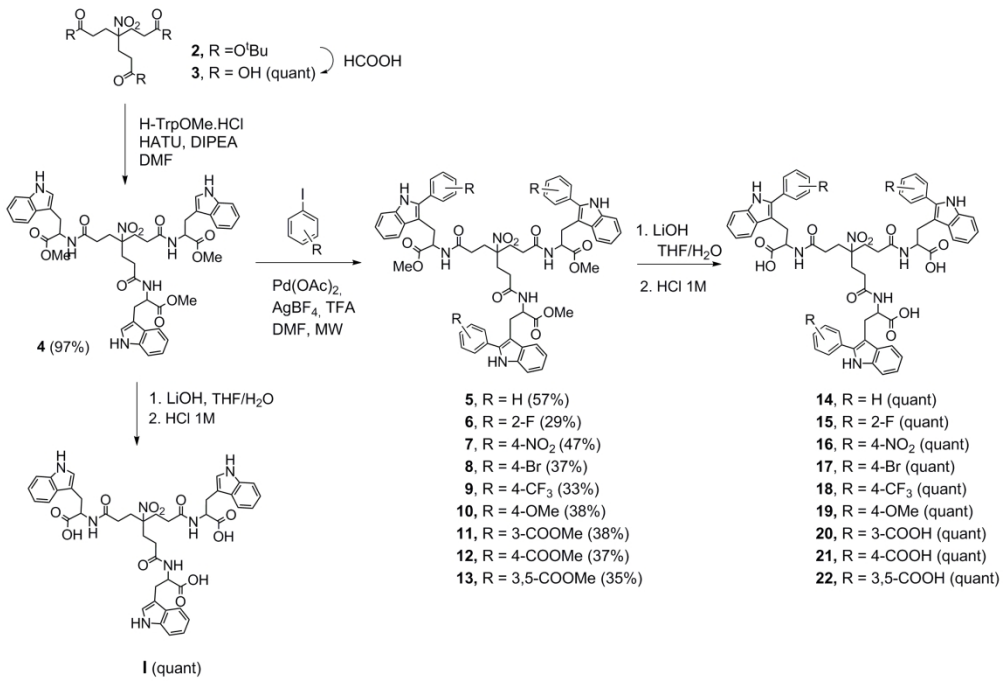

Scheme 1. Synthesis of the tripodal derivatives I and 14-22.

225x152mm (300 x 300 DPI)

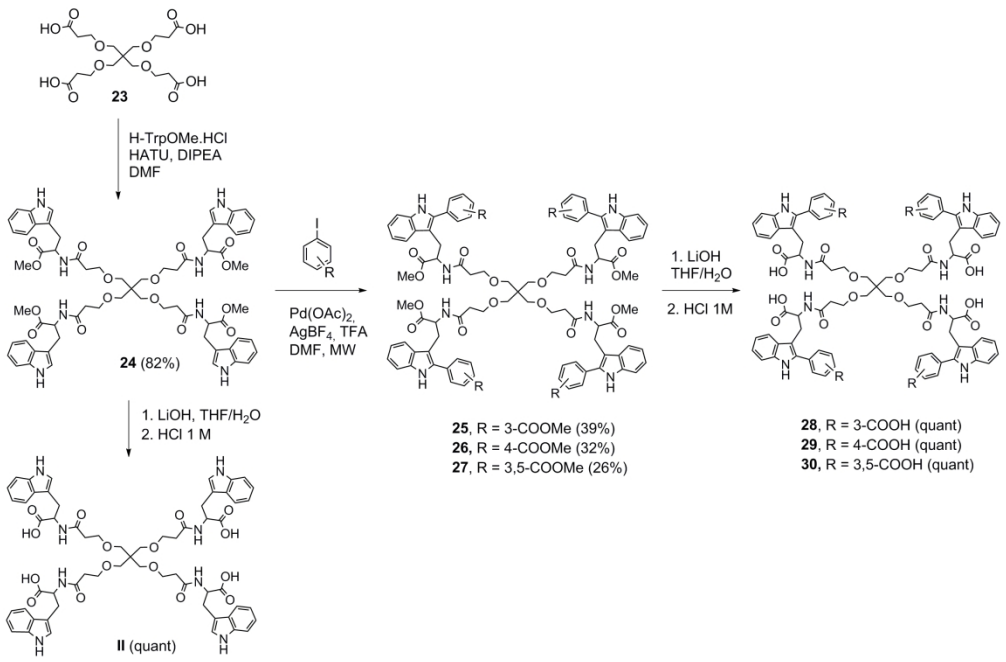

Scheme 2. Synthesis of the tetrapodal derivatives II and 28-30.

250x164mm (300 x 300 DPI)

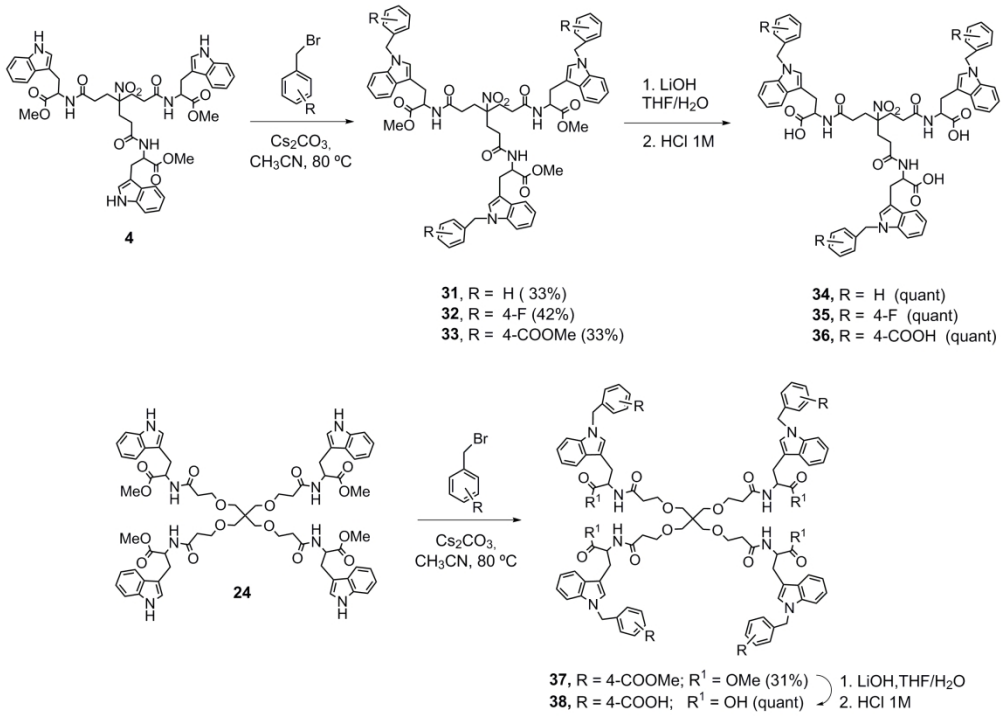

Scheme 3. Synthesis of the N1 substituted tripodal (34-36) and tetrapodal (38) derivatives.

240x171mm (300 x 300 DPI)

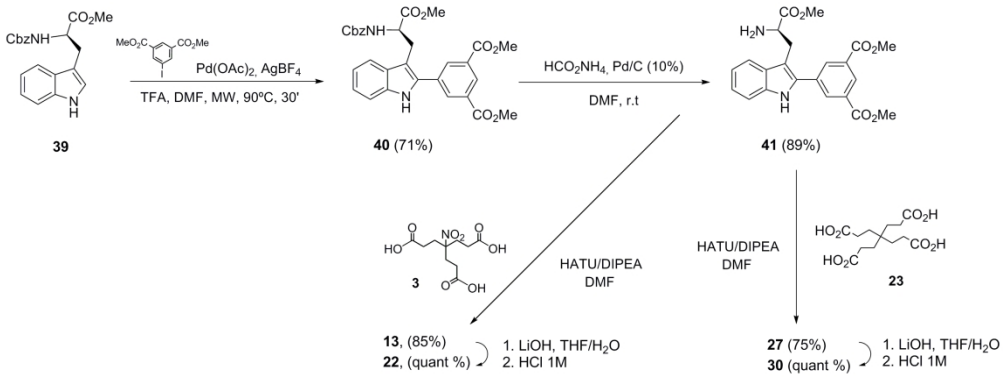

Scheme 4. Alternative synthetic route for the synthesis of 22 and 30.

243x91mm (300 x 300 DPI)